
This is an electronic reprint of the original article.
This reprint may differ from the original in pagination and typographic detail.

Manninen, Juuso; Haque, Mohammad Tasnimul; Vitali, David; Hakonen, Pertti
Enhancement of the optomechanical coupling and Kerr nonlinearity using the Josephson capacitance of a Cooper-pair box

Published in:
Physical Review B

DOI:
[10.1103/PhysRevB.105.144508](https://doi.org/10.1103/PhysRevB.105.144508)

Published: 01/04/2022

Document Version
Publisher's PDF, also known as Version of record

Please cite the original version:
Manninen, J., Haque, M. T., Vitali, D., & Hakonen, P. (2022). Enhancement of the optomechanical coupling and Kerr nonlinearity using the Josephson capacitance of a Cooper-pair box. *Physical Review B*, 105(14), 1-15. Article 144508. <https://doi.org/10.1103/PhysRevB.105.144508>

This material is protected by copyright and other intellectual property rights, and duplication or sale of all or part of any of the repository collections is not permitted, except that material may be duplicated by you for your research use or educational purposes in electronic or print form. You must obtain permission for any other use. Electronic or print copies may not be offered, whether for sale or otherwise to anyone who is not an authorised user.

Enhancement of the optomechanical coupling and Kerr nonlinearity using the Josephson capacitance of a Cooper-pair box

Juuso Manninen ¹, Mohammad Tasnimul Haque ¹, David Vitali ² and Pertti Hakonen ^{1,3}

¹*Low Temperature Laboratory, Department of Applied Physics, Aalto University, P.O. Box 15100, FI-00076 Espoo, Finland*

²*School of Science and Technology, Physics Division, University of Camerino, I-62032 Camerino (MC), Italy*

³*QTF Centre of Excellence, Department of Applied Physics, Aalto University, P.O. Box 15100, FI-00076 Aalto, Finland*



(Received 10 January 2021; revised 31 March 2022; accepted 31 March 2022; published 25 April 2022)

We propose a scheme for enhancing the optomechanical coupling between microwave and mechanical resonators by up to seven orders of magnitude to the ultrastrong coupling limit in a circuit optomechanical setting. The tripartite system considered here consists of a Josephson junction Cooper-pair box that mediates the coupling between the microwave cavity and the mechanical resonator. The optomechanical coupling can be modified by tuning the gate charge and the magnetic flux bias of the Cooper-pair box which in turn affect the Josephson capacitance of the Cooper-pair box. We additionally show that with a suitable choice of tuning parameters, the optomechanical coupling vanishes and the system purely exhibits a cross-Kerr type of nonlinearity between the cavity and the mechanical resonator. This allows the system to be used for phonon counting.

DOI: [10.1103/PhysRevB.105.144508](https://doi.org/10.1103/PhysRevB.105.144508)

I. INTRODUCTION

Cavity optomechanics [1] using superconducting microwave circuits [2–6] is an emerging platform for studies of macroscopic quantum phenomena. In particular, there is growing research interest in the ultrastrong coupling regime [7–13], where the strength of the single-photon optomechanical coupling is comparable to the resonant frequency of the mechanical resonator. Optomechanical coupling arises from the radiation pressure force acting on a mechanical resonator and, in the microwave regime, this radiation pressure coupling is intrinsically weak. The weak coupling can be amplified by applying a strong coherent pump to the cavity which linearizes the interaction between the cavity and the mechanical resonator. In the linear interaction limit, the quantum effects are observable only close to the quantum zero point fluctuations. However, a nonlinearity can be introduced into the system and a single-photon strong coupling regime can be reached allowing rich quantum physics experiments, e.g., preparing nonclassical states of light and mechanical resonators [14–18] for potential quantum information processing applications.

In the superconducting circuit architecture [19], several types of configurations have been proposed to add nonlinearities into the system such as a transmon qubit [20], SQUID [21], quantum capacitance of a nanotube in Coulomb blockade regime [22], and Josephson inductance [23,24], which has also been experimentally realized [25]. We propose to employ the Josephson Capacitance of the Cooper-pair box (CPB), which is dual to the operation of Josephson inductance as the nonlinear element for enhancing the optomechanical coupling. Looking from the gate electrode, a CPB can act as a nonlinear capacitive element known as the Josephson capacitance. This capacitance originates from the curvature of the energy bands of the CPB with respect to gate charge [26–30]. Josephson capacitance has been proposed to be utilized as a very sensitive phase detector [31] and a pair-breaking ra-

diation detector [32]. Here, we consider a tripartite system consisting of a microwave cavity, a CPB, and a mechanically movable capacitance. The coupling between the cavity and the mechanical resonator is mediated by the Josephson capacitance of the CPB and can be tuned by the charge and flux bias of the CPB. We show that with suitably tuned, realistic experimental parameters, the optomechanical coupling can be enhanced by seven orders of magnitude compared to direct optomechanical coupling without the presence of CPB, reaching the ultrastrong coupling regime.

In addition to boosting the optomechanical coupling, a cross-Kerr (CK)-type nonlinearity between the cavity and the mechanics is also formed amidst other nonlinear terms in the system Hamiltonian. The CK coupling $g_{CK}\hat{n}_a\hat{n}_b$ between two resonators a and b, with number operators \hat{n}_a and \hat{n}_b , can be used for quantum nondemolition measurements of number of quanta in one of the resonators since it directly affects the resonance frequency of the readout resonator [33]. In recent years, CK coupling in optomechanical systems has attracted theoretical interest [34–37], including a recent scheme to enhance the coupling to the order of the cavity linewidth [38]. Tunable CK interaction has been experimentally demonstrated for superconducting microwave circuits [39].

II. DESCRIPTION OF THE SYSTEM

A circuit diagram of the setup is presented in Fig. 1. The CPB formed of two Josephson junctions (JJs) with Josephson energies E_{J1}, E_{J2} and capacitances C_{J1}, C_{J2} couples a mechanical displacement dependent gate capacitance $C_{g1}(x)$ to a superconducting microwave cavity, modeled as a simple LC oscillator in a bias-T configuration. Here, we assume $C_{g1}(x) = C_{g10} + \frac{\partial C_{g1}(x)}{\partial x}x + \frac{1}{2}\frac{\partial^2 C_{g1}(x)}{\partial x^2}x^2$, where the derivatives are approximated for a parallel plate capacitor. This configuration allows the CPB to act as a capacitive element and,

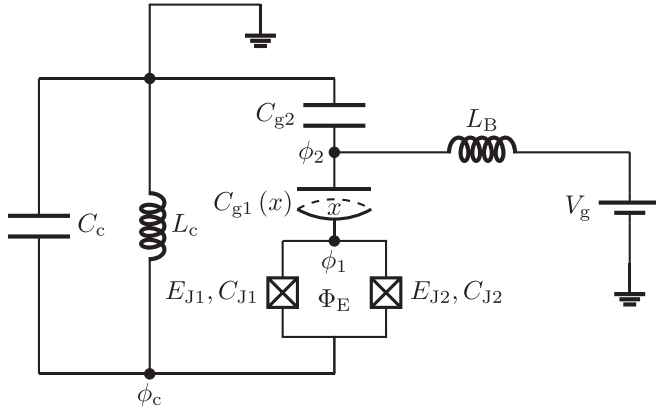


FIG. 1. Circuit diagram of the investigated optomechanical setup with the gate capacitance of the Cooper-pair box connected in parallel to the microwave cavity capacitance. The elements in the circuit are described in the text.

additionally, blocks the DC gate bias from entering into the microwave cavity and prevents the AC signal leaking out through the DC gate. The inductor L_B in the bias-T and the capacitor C_{g2} have impedances such that they do not affect the qubit dynamics. The junction capacitances C_{J1} and C_{J2} and the static part of the gate capacitance give the total single electron charging energy of the qubit, $E_C = e^2/2(C_{g10} + C_{J1} + C_{J2})$. Tunneling of a Cooper pair into the qubit island is tunable by the static gate charge given by the number of Cooper pairs in the island $n_{g0} = -V_g C_{g10}/(2e)$, where V_g is the gate voltage. Furthermore, the CPB is split and hence, by applying a magnetic flux Φ_E to the superconducting loop, the Josephson energy of the qubit can be controlled.

To better illustrate the procedure of deriving the effective Hamiltonian for the system, we assume in the following, without loss of generality, that the Josephson energies of the two junctions are equal, i.e., $E_{J1} = E_{J2} = E_J/2$, in which case the Hamiltonian of the unperturbed qubit is

$$\hat{H}_{\text{QB}} = -\frac{1}{2}(B_1\sigma_x + B_3\sigma_z), \quad (1)$$

with the ground-state energy, $E_{\text{GS}} = -\sqrt{B_1^2 + B_3^2}/2 = -B/2$, where $B_1 = E_J \cos(\pi \frac{\Phi_E}{\Phi_0})$ and $B_3 = -4E_C(1 - 2\delta n_{g0})$. Here $\sigma_{x(z)}$ is the first (third) Pauli spin matrix and $\Phi_0 = h/2e$ is the flux quantum and $\delta n_{g0} \in [0, 1]$ is the deviation from the two lowest charge states $|\text{int}(n_{g0})\rangle = |0\rangle$ and $|\text{int}(n_{g0}) + 1\rangle = |1\rangle$ determining the qubit. In principle, the junction energies can be different and the explicit full calculations of the system dynamics are presented in the Appendices.

III. CIRCUIT MODEL

Enhancement of the radiation pressure coupling can be understood from the quantum capacitance picture where the effective capacitance of the CPB is affecting the total capacitance of the cavity. For band k of the CPB, the effective capacitance is given by [28,29]

$$C_{\text{eff}}^k = \frac{C_{g1}C_J}{C_{g1} + C_J} - \frac{C_{g1}^2}{4e^2} \frac{\partial^2 E_k(\Phi_E, n_g)}{\partial n_g^2}, \quad (2)$$

where we denote $C_J = C_{J1} + C_{J2}$.

This effective capacitance C_{eff} , containing both geometric and quantum capacitance contributions of the CPB, is in parallel with the cavity capacitance C_c . As a consistency check, one sees that in the limit of small Josephson energy the effective capacitance approaches the geometric gate capacitance. The resonance frequency of the cavity is then $\omega_c = 1/\sqrt{L_c C_{\text{tot}}}$, where the total capacitance consist of the cavity capacitance in parallel with the second gate capacitance and the effective CPB capacitance, i.e., $C_{\text{tot}} = C_c + (\frac{1}{C_{g2}} + \frac{1}{C_{\text{eff}}})^{-1}$. The radiation pressure coupling is given by the linear expansion of the resonant frequency with respect to the mechanical displacement

$$\hbar g_{\text{rp}} = -\hbar \frac{\partial \omega_c}{\partial x} x_{\text{zp}}, \quad (3)$$

where x_{zp} is the zero point motion of the mechanical displacement.

A straightforward calculation yields

$$\frac{\partial \omega_c}{\partial x} = -\frac{1}{2} \frac{C_{g2}^2}{(C_{g2} + C_{\text{eff}})^2} \frac{\omega_c}{C_{\text{tot}}} \frac{\partial C_{\text{eff}}}{\partial x}, \quad (4a)$$

$$\begin{aligned} \frac{\partial C_{\text{eff}}}{\partial x} &= \frac{C_J C_{g1}'}{(C_{g1} + C_J)^2} - \frac{C_{g1} C_{g1}'}{2e^2} \frac{\partial^2 E_k}{\partial n_g^2} \\ &\quad - \frac{C_{g1}^2}{4e^2} \frac{\partial}{\partial x} \left(\frac{\partial^2 E_k}{\partial n_g^2} \right), \end{aligned} \quad (4b)$$

with $\frac{\partial}{\partial x} \left(\frac{\partial^2 E_k}{\partial n_g^2} \right) = \frac{\partial n_g}{\partial x} \frac{\partial}{\partial n_g} \left(\frac{\partial^2 E_k}{\partial n_g^2} \right)$ where $\frac{\partial n_g}{\partial x} = -\frac{C_{g1}'}{2e} V_g$.

Plugging Eqs. (4a) and (4b) into Eq. (3), we obtain the final expression for optomechanical coupling:

$$\begin{aligned} \hbar g_{\text{rp}} &= \hbar x_{\text{zp}} \left[\frac{1}{2} \frac{C_{g2}^2}{(C_{g2} + C_{\text{eff}})^2} \frac{\omega_c}{C_{\text{tot}}} \right] \\ &\quad \times \left[\frac{C_J C_{g1}'}{(C_{g1} + C_J)^2} - \frac{C_{g1} C_{g1}'}{2e^2} \frac{\partial^2 E_k}{\partial n_g^2} + \frac{C_{g1}^2 C_{g1}'}{8e^3} V_g \frac{\partial^3 E_k}{\partial n_g^3} \right]. \end{aligned} \quad (5)$$

The enhancement of the radiation pressure coupling is compared to the direct optomechanical coupling in the absence of the qubit

$$g_0 = -\frac{1}{2} \frac{C_{g2}^2}{(C_{g1} + C_{g2})^2} \frac{\omega_c}{C_d} C_{g1}' x_{\text{zp}}, \quad (6)$$

where the cavity frequency is influenced by the total capacitance $C_d = C_c + \frac{C_{g1} C_{g2}}{C_{g1} + C_{g2}}$ in the direct coupling scheme.

For a numerical estimation of the radiation pressure coupling, presented in Fig. 2(a), we choose a cavity of resonant frequency $\omega_c/2\pi = 5$ GHz with characteristic impedance $Z_0 = 100 \Omega$ resulting in capacitance $C_c = 0.318$ pF and inductance $L_c = 3.18$ nH. The other parameter values chosen are $V_g = 10$ V, $E_C/h = 18$ GHz ($\sim 74 \mu\text{eV}$), $E_J/h = 3$ GHz ($\sim 12 \mu\text{eV}$), thus $E_J/E_C = 1/6$. The reason to choose these values for E_C , E_J is to minimize quasiparticle poisoning which is a well known limiting factor associated with CPB devices. The band energies of CPB are $2e$ periodic with respect to gate charge modulation. In practice, however, due to tunneling of nonequilibrium quasiparticles on and off the

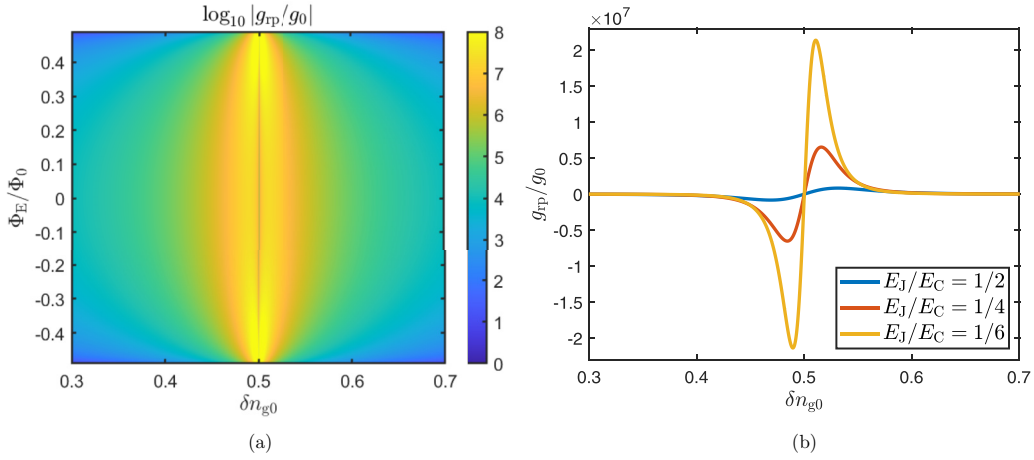


FIG. 2. (a) The enhancement of the optomechanical radiation pressure coupling g_{rp} due to the quantum capacitance compared to direct coupling g_0 as a function of flux bias and gate charge. Here $E_C/h = 18$ GHz and $E_J/h = 3$ GHz. (b) The enhancement of the radiation pressure coupling for different E_J/E_C ratios as a function of gate charge with $E_J/h = 3$ GHz at $\Phi_E = 0$.

CPB island [40,41], the periodicity can change from $2e$ to $1e$. To reduce this effect, it is desirable to have E_C smaller than the superconducting energy gap Δ_g . Typically, qubits are made of superconducting Aluminum (Al) junctions and for Al, critical current (T_C) is 1.2 K, the superconducting gap $\Delta_g \sim 1.76k_B T_C \sim 182 \mu eV$, which is well above the chosen value.

Another crucial factor that influences the coupling strength is the E_J/E_C ratio. In Fig. 2(b), we plot the coupling enhancement g_{rp}/g_0 against gate charge n_g for several E_J/E_C ratios at flux $\Phi_E = 0$ to better illustrate how the enhancement depends on n_g . The maximum coupling is reachable near the charge qubit limit $E_C \gg E_J$.

As depicted below in the quantum mechanical treatment of the circuit, Eq. (22), the device exhibits a CK type of nonlinearity $g_{CK}a^\dagger a(b^\dagger + b)^2$. We do not use here the typical quantum optics expression given by the product of number operators because in the strong coupling regime where g_{CK} is comparable to the mechanical frequency, the $b^2 + \text{H.c.}$ term

is not negligible. Using the quantum capacitance approach similar to deriving Eq. (5), we obtain the CK coupling

$$\hbar g_{CK} = \frac{1}{2} \hbar \frac{\partial^2 \omega_c}{\partial x^2} x_{zp}^2, \quad (7)$$

where the second-order derivative of the cavity frequency is

$$\begin{aligned} \frac{\partial^2 \omega_c}{\partial x^2} &= \frac{1}{4} \omega_c C_{g2}^2 \left(\frac{\partial C_{\text{eff}}}{\partial x} \right)^2 \\ &\times \frac{C_{g2}(4C_c + 3C_{g2}) + 4(C_c + C_{g2})C_{\text{eff}}}{(C_{g2} + C_{\text{eff}})^2 [C_c C_{g2} + (C_c + C_{g2})C_{\text{eff}}]^2} \\ &- \frac{1}{2} \omega_c C_{g2}^2 \frac{\partial^2 C_{\text{eff}}}{\partial x^2} \\ &\times \frac{1}{(C_{g2} + C_{\text{eff}})[C_c C_{g2} + (C_c + C_{g2})C_{\text{eff}}]}, \quad (8) \end{aligned}$$

with

$$\begin{aligned} \frac{\partial^2 C_{\text{eff}}}{\partial x^2} &= -\frac{C_J C_{g1}^{\prime 2}}{(C_{g1} + C_J)^2} + \frac{C_J C_{g1}^{\prime\prime}}{C_{g1} + C_J} + C_J C_{g1} \left[\frac{2C_{g1}^{\prime 2}}{(C_{g1} + C_J)^3} - \frac{C_{g1}^{\prime\prime}}{(C_{g1} + C_J)^2} \right] \\ &- \frac{1}{4e^2} \left\{ (2C_{g1}^{\prime 2} + 2C_{g1} C_{g1}^{\prime\prime}) \frac{\partial^2 E_k}{\partial n_g^2} - \left(2C_{g1} C_{g1}^{\prime 2} \frac{V_g}{e} + C_{g1}^2 C_{g1}^{\prime\prime} \frac{V_g}{2e} \right) \frac{\partial^3 E_k}{\partial n_g^3} + C_{g1}^2 \left(-\frac{V_g C_{g1}^{\prime}}{2e} \right)^2 \frac{\partial^4 E_k}{\partial n_g^4} \right\}. \quad (9) \end{aligned}$$

Noticeably, the radiation pressure coupling is antisymmetrical with respect to the degeneracy point $\delta n_{g0} = 1/2$, whereas the CK coupling is completely symmetrical in this sense and, additionally, the radiation pressure vanishes when the gate charge is tuned to the degeneracy point of the qubit, as shown in Figs. 2(a) and 2(b). However, the CK term does not vanish at this point, see Figs. 3(a) and 3(a). By choosing $E_J/E_C \ll 1$ and detuning very close to charge degeneracy point, we are able to achieve a very strong Kerr nonlinearity without the optomechanical radiation pressure coupling. Therefore, with a proper choice of the gate charge and detuning, the system

can be described with a simple Hamiltonian

$$\hat{H}_{CK} = \hbar \omega_c \hat{a}^\dagger \hat{a} + \hbar \omega_m \hat{b}^\dagger \hat{b} + \hbar g_{CK} \hat{a}^\dagger \hat{a} (\hat{b}^\dagger + \hat{b})^2. \quad (10)$$

Looking at Eq. (10), the cavity resonant frequency is starkly shifted due to the number of phonons in the mechanical part, since with proper parameter selection the maximum predicted g_{CK} can reach up to typical microwave cavity linewidth $\kappa \sim 2\pi \times 1 - 10$ MHz [5,25]. This allows the system to function as a very good phonon counter with the cavity as the readout.

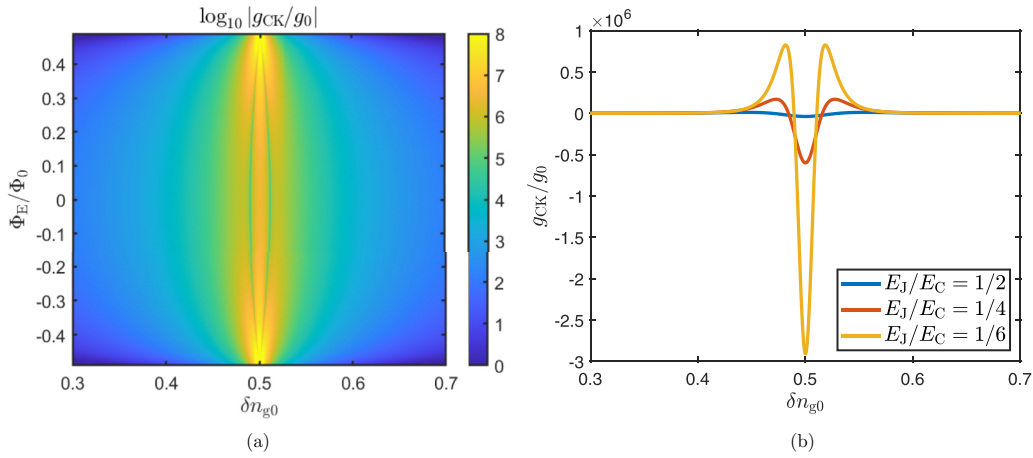


FIG. 3. (a) The CK coupling g_{CK} , scaled by g_0 , arising from the circuit quantum capacitance calculations as a function of flux bias and gate charge. Here $E_C/h = 18$ GHz and $E_J/h = 3$ GHz. (b) The scaled CK coupling for different E_J/E_C ratios with $E_J/h = 3$ GHz at $\Phi_E = 0$.

IV. PERTURBATIVE QUANTUM MECHANICS APPROACH

Here we consider the dynamics of the system with a fully quantum mechanical treatment. This approach better highlights the involvement of the qubit to the enhancement of the cavity-mechanics coupling. In the above circuit model, the quantum capacitance of the Josephson junctions is seen to affect the total capacitance felt by the cavity, whereas here the coupling is seen to arise from a direct perturbation of the cavity and the mechanics on the qubit.

Naturally, the cavity and the mechanics can be considered as harmonic oscillators with Hamiltonians

$$\hat{\mathcal{H}}_c = \hbar\omega_c \hat{a}^\dagger \hat{a}, \quad (11a)$$

$$\hat{\mathcal{H}}_m = \hbar\omega_m \hat{b}^\dagger \hat{b}. \quad (11b)$$

Here $\hat{a}^{(\dagger)}$ and $\hat{b}^{(\dagger)}$ are the annihilation (creation) operators of the cavity photons and the phonons in the moving capacitor, respectively, and we have neglected some terms arising from the detailed derivation provided in Appendix D, since these terms do not contribute to the radiation pressure and CK couplings.

Note that here the cavity frequency ω_c is position dependent. A straightforward calculation yields the direct radiation pressure and CK couplings from the quantum mechanical model

$$\tilde{g}_{\text{rpd}} = \frac{\omega_{c0}}{2C_{\Sigma c}} \frac{C_J^2 C'_{g1}}{(C_J + C_{g1})^2} x_{\text{zpd}}, \quad (12a)$$

$$\begin{aligned} \tilde{g}_{\text{CKd}} &= \frac{1}{2}\omega_{c0} \left[\frac{3}{4C_{\Sigma c}^2} \left(\frac{C_J^2 C'_{g1}}{(C_J + C_{g1})^2} \right)^2 - \frac{C_J^2}{2C_{\Sigma c}} \right. \\ &\quad \left. \times \left(\frac{-2C_{g1}^2 + (C_J + C_{g1})C''_{g1}}{(C_J + C_{g1})^3} \right) \right] x_{\text{zpd}}^2, \end{aligned} \quad (12b)$$

with $C_{\Sigma c} = C_c + \frac{C_{g1}C_J}{C_{g1}+C_J}$. We denote the optomechanical couplings arising from quantum mechanical model with superscript \sim to distinguish them from the circuit model couplings. The full derivation is in Appendix D.

The charging energy Hamiltonian of the qubit in the charge basis, expressed with the number of Cooper pairs, is

$$\hat{\mathcal{H}}_{\text{ch}} = 4E_C \sum_n (\hat{n} - n_g(x))^2 |n\rangle \langle n|. \quad (13)$$

Here AC effects arising from the cavity oscillations are ignored.

Considering the two lowest Cooper pair charge states $|\text{int}(n_{g0})\rangle$ and $|\text{int}(n_{g0}) + 1\rangle$ as the ground state and excited states, $|0\rangle$ and $|1\rangle$, respectively, the charging energy Hamiltonian in the two-level system approximation becomes

$$\hat{\mathcal{H}}_{\text{ch}} = -\frac{B_3}{2}\sigma_z - g_m \hat{x}_m \sigma_z, \quad (14)$$

where the following shorthand notation is used:

$$g_m = 4E_C \frac{\partial n_g}{\partial x} x_{\text{zpd}} = 4E_C \left(-\frac{1}{2e} C'_{g1} V_g \right) x_{\text{zpd}}, \quad (15a)$$

$$\hat{x}_m = \hat{b} + \hat{b}^\dagger. \quad (15b)$$

Here, σ_x , σ_y , σ_z are Pauli matrices acting on the space spanned by states $|0\rangle$ and $|1\rangle$, and $\hat{a}^{(\dagger)}$. The first term gives the unperturbed qubit excitation energy, and the second arises from the charge fluctuations $\delta n_g = \frac{\partial C_{g1}}{\partial x} \hat{x}$.

The node fluxes on the cavity side of the Josephson junctions and on the qubit island are ϕ_c and ϕ_1 , respectively. The tunneling energy Hamiltonian is thus

$$\begin{aligned} \mathcal{H}_{\text{JJ}} &= -E_{J1} \cos \left(2\pi \frac{\phi_1 - \phi_c + \frac{1}{2}\Phi_E}{\Phi_0} \right) \\ &\quad - E_{J2} \cos \left(2\pi \frac{\phi_1 - \phi_c - \frac{1}{2}\Phi_E}{\Phi_0} \right) \\ &= -E_J \cos \left(\pi \frac{\Phi_E}{\Phi_0} \right) \left[\cos \left(2\pi \frac{\phi_1}{\Phi_0} \right) \cos \left(2\pi \frac{\phi_c}{\Phi_0} \right) \right. \\ &\quad \left. + \sin \left(2\pi \frac{\phi_1}{\Phi_0} \right) \sin \left(2\pi \frac{\phi_c}{\Phi_0} \right) \right], \end{aligned} \quad (16)$$

where symmetrical Josephson junctions (JJs) are assumed. The following results are all written assuming $E_{J1} = E_{J2} = E_J/2$ for simplicity, and the full formulas are presented in the Appendices.

In general, a node flux can be related to the phase of the node with $\varphi_i = 2\pi \frac{\phi_i}{\Phi_0}$. One can show that the quantized phase of the cavity node can be tied to the annihilation (creation) operator of photons $\hat{a}^{(\dagger)}$ so $\hat{\varphi}_c = \eta(\hat{a} + \hat{a}^\dagger)$, where $\eta = \sqrt{2e^2 Z_0 / \hbar}$ with $Z_0 = \sqrt{L_c / C_c}$. The approximations in the quantum mechanical calculation rely on $\eta \ll 1$. The conjugate variable of the cavity flux, the cavity charge is similarly defined $\hat{Q}_c = -iQ_{zp}(\hat{a} - \hat{a}^\dagger)$, where the zero-point motion of charge is $Q_{zp} = \sqrt{\frac{\hbar}{2Z_0}}$. See Appendix D for the derivations.

The cavity-qubit coupling parameter $\eta \ll 1$ for typical microwave cavities. Therefore, we can now expand the sine and cosine terms of $\hat{\varphi}_c$ in Eq. (16) up to second order in η . Properties of the phase operators also allow us to identify the superconducting phase of the island with ladder operators in the effective qubit so considering on states $|0\rangle$ and $|1\rangle$, we obtain $\cos(\hat{\varphi}_1) \mapsto \sigma_x/2$ and $\sin(\hat{\varphi}_1) \mapsto -\sigma_y/2$, see Appendix D for derivation. The approximate quantized Hamiltonian for the Josephson junctions is thus

$$\hat{H}_{JJ} = -\frac{B_1}{2}\sigma_x + g_1\sigma_y\hat{x}_c + g_2\sigma_x\hat{x}_c^2, \quad (17)$$

with $g_1 = B_1\eta/2$, $g_2 = B_1\eta^2/4$, and $\hat{x}_c = \hat{a} + \hat{a}^\dagger$.

Let us decompose the Hamiltonians Eqs. (14) and (17) into parts with the different Pauli matrices and write the full system Hamiltonian

$$\hat{H} = \hat{H}_c + \hat{H}_m - \frac{1}{2}(\tilde{B}_1\sigma_x + \tilde{B}_2\sigma_y + \tilde{B}_3\sigma_z), \quad (18)$$

with the perturbed qubit terms

$$\tilde{B}_1 = B_1 - 2g_2\hat{x}_c^2, \quad (19a)$$

$$\tilde{B}_2 = -2g_1\hat{x}_c, \quad (19b)$$

$$\tilde{B}_3 = B_3 + 2g_m\hat{x}_m. \quad (19c)$$

The Hamiltonian Eq. (18) can thus be interpreted as the cavity and the mechanics slightly perturbing the isolated qubit parameters $B_{1,2,3}$ ($B_2 = 0$ for symmetrical JJs). In other words, the qubit mediates the interaction between the cavity and the mechanics leading to a notable enhancement of the coupling.

Let us consider a perturbative approach to solving the cavity-mechanics couplings from Eq. (18) and note that the eigenenergies of a qubit with Hamiltonian $-\frac{1}{2}(\tilde{B}_1\sigma_x + \tilde{B}_2\sigma_y + \tilde{B}_3\sigma_z)$ are $\pm\frac{1}{2}\sqrt{\tilde{B}_1^2 + \tilde{B}_2^2 + \tilde{B}_3^2}$. We write the Hamiltonian Eq. (18) in terms of its ground state

$$\begin{aligned} \hat{H} &= \hat{H}_c + \hat{H}_m - \frac{1}{2}\sqrt{\tilde{B}_1^2 + \tilde{B}_2^2 + \tilde{B}_3^2} \\ &= \hat{H}_c + \hat{H}_m - \frac{1}{2}B\sqrt{1 + \frac{1}{B^2}(\delta\hat{x}_c^4 + \epsilon\hat{x}_m + \lambda\hat{x}_m^2)}, \end{aligned} \quad (20)$$

with

$$B = \sqrt{B_1^2 + B_3^2}, \quad (21a)$$

$$\delta = 4g_2^2, \quad (21b)$$

$$\epsilon = 4B_3g_m, \quad (21c)$$

$$\lambda = 4g_m^2. \quad (21d)$$

We can expand the square-root term as $\sqrt{1+x} \approx 1 + \frac{x}{2} - \frac{x^2}{8} + \frac{x^3}{16}$, and we note that the expansion is more accurate further away from the degeneracy point of the qubit, where B is larger. This technique yields cavity-mechanics couplings that approach the ones obtained from the circuit model far away from the degeneracy point when $E_J \ll E_C$.

Up to the third order in the expansion, we obtain

$$\begin{aligned} & -\frac{1}{2}\sqrt{\tilde{B}_1^2 + \tilde{B}_2^2 + \tilde{B}_3^2} \\ & \approx -\frac{1}{2}B - \frac{1}{4B}(\delta\hat{x}_c^4 + \epsilon\hat{x}_m + \lambda\hat{x}_m^2) \\ & + \frac{1}{16B^3}(\delta\hat{x}_c^4 + \epsilon\hat{x}_m + \lambda\hat{x}_m^2)^2 \\ & - \frac{1}{32B^5}(\delta\hat{x}_c^4 + \epsilon\hat{x}_m + \lambda\hat{x}_m^2)^3, \end{aligned} \quad (22)$$

where, after normal ordering the cavity and mechanics operators, we identify the radiation pressure coupling as the prefactor of the term $-\hbar g_{rp}\hat{a}^\dagger\hat{a}(\hat{b}^\dagger + \hat{b})$,

$$\hbar\tilde{g}_{rp} = \frac{\delta\epsilon}{4B^5}\{-6B^2 + 315\delta + 27\lambda\}, \quad (23)$$

and the CK coupling as the prefactor of the term $\hbar g_{CK}\hat{a}^\dagger\hat{a}(\hat{b} + \hat{b}^\dagger)^2$:

$$\hbar\tilde{g}_{CKp} = -\frac{1}{2}\frac{\delta}{8B^5}\{-24B^2\lambda + 1260\delta\lambda + 18\epsilon^2 + 108\lambda^2\}. \quad (24)$$

The complete radiation pressure coupling from the quantum mechanical calculation is the sum of the direct coupling Eq. (12a) and the qubit mediated coupling Eq. (23) $\tilde{g}_{rp} = \tilde{g}_{rpd} + \tilde{g}_{rpp}$. Similarly, Eqs. (12b) and (24) give the full CK coupling $\tilde{g}_{CK} = \tilde{g}_{CKd} + \tilde{g}_{CKp}$.

The circuit and quantum mechanical descriptions of the system dynamics agree qualitatively but have differences quantitatively close to the degeneracy point of the qubit due to the inaccuracy of the perturbative quantum mechanical approach in that regime. However, importantly, the circuit and quantum mechanical models align perfectly in the limit $E_J \rightarrow 0$ and, additionally, good agreement is found far away from the degeneracy point for small E_J , Z_0 , and V_g . Better agreement is also naturally obtained by going to higher orders in the expansion of the $-\frac{1}{2}\sqrt{\tilde{B}_1^2 + \tilde{B}_2^2 + \tilde{B}_3^2}$ term. A major reason for the quantitative differences between the different approaches is that the classical circuit theory takes into account only the change in the gate voltage while the quantum mechanical theory also includes the change in the phase across the Josephson junctions in the CPB. Thus, the QM model in fact mixes the quantum capacitance response (V_g change) and the Josephson inductance response (phase change). The relevance of the mixing depends on the parameters, which makes an overall estimation of the influence of this effect difficult. This effect becomes larger when reducing E_J , which clarifies why the agreement at low E_J is not achieved as well as expected when E_J/E_C is reduced, even though ultimately at $E_J = 0$ a perfect agreement is met. In Appendix E, we present the full derivation of these couplings. An important agreement of the two descriptions is also that, at the degeneracy point, the radiation pressure coupling vanishes and the CK coupling

obtains a large nonzero value enabling a rich platform for phonon counting experiments.

V. DISCUSSION

We are interested in reaching the ultrastrong single-photon coupling regime $g_{\text{rp}} > \omega_m$, where one can observe the intrinsic nonlinearity of optomechanical coupling that goes unseen for weaker couplings that allow the linearization of the interaction. With our scheme, we are able to obtain a radiation pressure coupling enhancement of seven orders of magnitude by utilizing the high range of tunability offered by the setup. With the proper selection of gate charge and the magnetic flux through the qubit loop, the desired coupling strength for a specific purpose can be obtained. Moreover, owing to the wide tuning options, one can find a regime with enhanced radiation pressure coupling and vanishing CK coupling or vice versa, which makes this setup practical for multiple types of studies.

For an optomechanical setup with a direct radiation pressure coupling g_0 of the order of 10 Hz, we are thus able to reach a coupling of the order of 100 MHz, which facilitates probing the ground state of a typical flexural nanomechanical resonator without the need for sideband cooling.

Above, we performed our model calculations for a cavity with impedance $Z_0 = 100 \Omega$, which means that the zero-point fluctuations of flux $\Phi_{z\text{p}} = \sqrt{\hbar Z_0/2}$ exceed the zero-point fluctuation of charge $Q_{z\text{p}} = \sqrt{\hbar/(2Z_0)}$, making the device characteristics more strongly influenced by flux than charge fluctuations. As seen in Figs. 2(a) and 3(a), the enhancement of the radiation pressure and CK couplings is more affected by changes in n_g than in Φ_E . With proper tuning of n_g , sizable enhancements to g_{rp} and g_{CK} can still be obtained even with averaging effects in Φ_E arising from large phase fluctuations.

In summary, we have analyzed an optomechanical setup based on utilization of Josephson (quantum) capacitance of a CPB to boost the optomechanical coupling. We reach an enhancement of radiation pressure by seven orders of magnitude, which brings the system well into the ultrastrong coupling regime. The coupling is highly tunable by charge and flux bias and, by proper selection of the bias point, strongly enhanced CK coupling without radiation pressure effects can be achieved for phonon-counting purposes.

ACKNOWLEDGMENTS

We thank Andreas Hüttel, Yuriy Makhlin, Francesco Massele, and Tero Heikkilä for useful discussions. This work was supported by the Academy of Finland Center of Excellence Quantum Technology Finland (Grant No. 312295) and RADESS program (Grant No. 314448, BOLOSE), as well as by the European Research Council (Grant No. 670743). M.T.H. acknowledges support from the European Union's Horizon 2020 program for research and innovation under Grant Agreement No. 722923 (Marie Curie ETN-OMT) and a three-month-long secondment at University of Camerino, during which part of the work was carried out. J.M. thanks the support of the Vilho, Yrjö and Kalle Väisälä Foundation of the Finnish Academy of Science and Letters. This work was also supported in part by COST Action CA16218 (NANOCOHYBRI) and the European Microkelvin Platform (EMP, No. 824109).

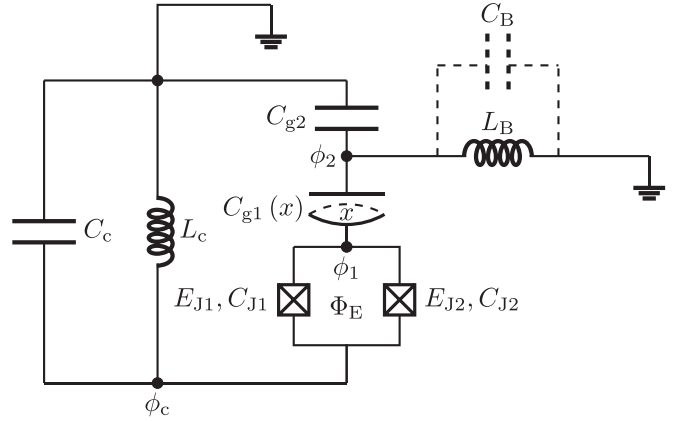


FIG. 4. Schematics of the Cooper-pair box circuit for enhancement of optomechanical coupling. For elements, see text.

APPENDIX A: FORMING THE HAMILTONIAN

We define the node flux at node i at time t as

$$\phi_i(t) = \int^t V_i(\tau) d\tau. \quad (\text{A1})$$

This implies that the voltage at node i can be expressed as

$$V_i(t) = \dot{\phi}_i. \quad (\text{A2})$$

The node flux is also related to the phase of the node with

$$\phi_i = 2\pi \frac{\phi_i}{\Phi_0}, \quad (\text{A3})$$

where $\Phi_0 = \frac{h}{2e}$ is the flux quantum. The node indices corresponding to each capacitive island of the circuit can be seen in Fig. 4.

The energy stored in the capacitive elements of the circuit is

$$\begin{aligned} \mathcal{T} = & \frac{C_J}{2} (\phi_1 - \phi_c)^2 + \frac{C_{g1}}{2} (\phi_1 - \phi_2)^2 \\ & + \frac{1}{2} (C_{g2} + C_B) \phi_2^2 + \frac{C_c}{2} \phi_c^2, \end{aligned} \quad (\text{A4})$$

where $C_J = C_{J1} + C_{J2}$ is the capacitance of the Josephson junctions, C_{g1} and C_{g2} the gate capacitances, and C_c the capacitance of the LC cavity. The position dependence of $C_{g1} = C_{g1}(x)$ is omitted for notational convenience. The bias capacitance C_B is included to induce a bias voltage onto island 2. After taking $C_B \rightarrow \infty$, the voltage on island 2 corresponds to the bias voltage. Detailed calculations are given below. Additionally, for the method of nodes to work, the net of the capacitive elements connecting all of the nodes of the circuit needs to be simply connected [42].

Similarly, the inductive energy of the system is

$$\begin{aligned} \mathcal{U} = & -E_{J1} \cos \left(2\pi \frac{\phi_1 - \phi_c + \frac{1}{2} \Phi_E}{\Phi_0} \right) \\ & - E_{J2} \cos \left(2\pi \frac{\phi_1 - \phi_c - \frac{1}{2} \Phi_E}{\Phi_0} \right) \\ & + \frac{1}{2L_B} \phi_2^2 + \frac{1}{2L_c} \phi_c^2. \end{aligned} \quad (\text{A5})$$

Here E_{J1} , E_{J2} are the Josephson energies of the junctions, Φ_E the external flux through the loop of the CPB, L_B the bias inductance, and L_c the inductance of the LC cavity.

The Lagrangian $\mathcal{L}(\phi_i, \dot{\phi}_i)$ is thus

$$\mathcal{L} = \mathcal{T} - \mathcal{U} = \frac{1}{2} \vec{\phi}^\top [C] \vec{\phi} - \mathcal{U}, \quad (\text{A6})$$

where

$$[C] = \begin{pmatrix} C_J + C_{g1} & -C_{g1} & -C_J \\ -C_{g1} & C_{g1} + C_{g2} + C_B & 0 \\ -C_J & 0 & C_c + C_J \end{pmatrix} \vec{\phi} = \begin{pmatrix} \dot{\phi}_1 \\ \dot{\phi}_2 \\ \dot{\phi}_c \end{pmatrix}. \quad (\text{A7})$$

Now the Hamiltonian of the system $\mathcal{H}(\phi_i, Q_i)$ can be expressed with the conjugate momenta

$$Q_i = \frac{\partial \mathcal{L}}{\partial \dot{\phi}_i} \quad (\text{A8})$$

that correspond to the electric charge on the island i . The canonical relation between the Lagrangian and the Hamiltonian gives

$$\begin{aligned} \mathcal{H} &= \sum_i \dot{\phi}_i \frac{\partial \mathcal{L}}{\partial \dot{\phi}_i} - \mathcal{L} = \sum_i \dot{\phi}_i Q_i - \mathcal{L} \\ &= \frac{1}{2} \vec{Q}^\top [C]^{-1} \vec{Q} + \mathcal{U}. \end{aligned} \quad (\text{A9})$$

Here, the inverse of the capacitance matrix is

$$[C]^{-1} = \begin{pmatrix} \frac{1}{C_{\Sigma 1}} & \frac{1}{C_{\Sigma 12}} & \frac{1}{C_{\Sigma 1c}} \\ \frac{1}{C_{\Sigma 12}} & \frac{1}{C_{\Sigma 2}} & \frac{1}{C_{\Sigma 2c}} \\ \frac{1}{C_{\Sigma 1c}} & \frac{1}{C_{\Sigma 2c}} & \frac{1}{C_{\Sigma c}} \end{pmatrix}, \quad (\text{A10})$$

with the following shorthand notations:

$$\frac{1}{C_{\Sigma 1}} = \frac{(C_c + C_J)(C_B + C_{g1} + C_{g2})}{C_c C_J (C_B + C_{g2}) + C_{g1} [C_c (C_B + C_{g2}) + C_J (C_B + C_c + C_{g2})]}, \quad (\text{A11a})$$

$$\frac{1}{C_{\Sigma 2}} = \frac{C_c C_J + C_{g1} (C_c + C_J)}{C_c C_J (C_B + C_{g2}) + C_{g1} [C_c (C_B + C_{g2}) + C_J (C_B + C_c + C_{g2})]}, \quad (\text{A11b})$$

$$\frac{1}{C_{\Sigma c}} = \frac{C_J (C_B + C_{g2}) + C_{g1} (C_B + C_{g2} + C_J)}{C_c C_J (C_B + C_{g2}) + C_{g1} [C_c (C_B + C_{g2}) + C_J (C_B + C_c + C_{g2})]}, \quad (\text{A11c})$$

$$\frac{1}{C_{\Sigma 12}} = \frac{C_{g1} (C_c + C_J)}{C_c C_J (C_B + C_{g2}) + C_{g1} [C_c (C_B + C_{g2}) + C_J (C_B + C_c + C_{g2})]}, \quad (\text{A11d})$$

$$\frac{1}{C_{\Sigma 1c}} = \frac{C_J (C_B + C_{g1} + C_{g2})}{C_c C_J (C_B + C_{g2}) + C_{g1} [C_c (C_B + C_{g2}) + C_J (C_B + C_c + C_{g2})]}, \quad (\text{A11e})$$

$$\frac{1}{C_{\Sigma 2c}} = \frac{C_{g1} C_J}{C_c C_J (C_B + C_{g2}) + C_{g1} [C_c (C_B + C_{g2}) + C_J (C_B + C_c + C_{g2})]}. \quad (\text{A11f})$$

Thus, the Hamiltonian can be written out explicitly

$$\mathcal{H} = \frac{1}{2C_{\Sigma 1}} Q_1^2 + \frac{1}{2C_{\Sigma 2}} Q_2^2 + \frac{1}{2C_{\Sigma c}} Q_c^2 + \frac{1}{C_{\Sigma 12}} Q_1 Q_2 + \frac{1}{C_{\Sigma 1c}} Q_1 Q_c + \frac{1}{C_{\Sigma 2c}} Q_2 Q_c + \mathcal{U}. \quad (\text{A12})$$

Define the nominal bias voltage

$$V_g = \frac{Q_2}{C_{\Sigma 2}} \quad (\text{A13})$$

and calculate the real voltage on island 2:

$$\frac{\partial \mathcal{H}}{\partial Q_2} = \frac{1}{C_{\Sigma 2}} Q_2 + \frac{1}{C_{\Sigma 12}} Q_1 + \frac{1}{C_{\Sigma 2c}} Q_c = V_g + \frac{1}{C_{\Sigma 12}} Q_1 + \frac{1}{C_{\Sigma 2c}} Q_c. \quad (\text{A14})$$

In the limit $C_B \rightarrow \infty$, we obtain $\frac{\partial \mathcal{H}}{\partial Q_2} = V_g$, i.e., island 2 is now set to a potential that can be tuned with V_g .

Define the charging energy of the CPB, the number of Cooper pairs on island 1, and the nominal gate charge:

$$E_C = \frac{e^2}{2C_{\Sigma 1}}, \quad (\text{A15a})$$

$$n = \frac{Q_1}{2e}, \quad (\text{A15b})$$

$$n_g = -\frac{1}{2e} \frac{C_{\Sigma 1} C_{\Sigma 2}}{C_{\Sigma 12}} V_g. \quad (\text{A15c})$$

With these definitions along with Eq. (A13), the Hamiltonian Eq. (A12) can be reformulated to a standard form

$$\mathcal{H} = 4E_C (n - n_g)^2 + 4E_C \left(\frac{C_{\Sigma 12}^2}{C_{\Sigma 1} C_{\Sigma 2}} - 1 \right) n_g^2 + \frac{1}{2C_{\Sigma c}} Q_c^2 + \left(\frac{1}{C_{\Sigma 1c}} \cdot 2en + \frac{C_{\Sigma 12}}{C_{\Sigma 1} C_{\Sigma 2c}} \cdot 2en_g \right) Q_c + \mathcal{U}. \quad (\text{A16})$$

Let us now focus on \mathcal{U} in Eq. (A5) and, specifically, the Josephson junction part of it. Let us define the Josephson energies of the junctions as

$$E_{J1} = (1 + d) \frac{E_J}{2}, \quad (\text{A17a})$$

$$E_{J2} = (1 - d) \frac{E_J}{2}, \quad (\text{A17b})$$

where $d \in [0, 1)$ describes the difference of the Josephson energies of the two junctions. Using Eq. (A17) and the identity $\cos(\alpha \pm \beta) = \cos \alpha \cos \beta \mp \sin \alpha \sin \beta$, we can rewrite

$$\begin{aligned} & -E_{J1} \cos\left(2\pi \frac{\phi_1 - \phi_c + \frac{1}{2}\Phi_E}{\Phi_0}\right) - E_{J2} \cos\left(2\pi \frac{\phi_1 - \phi_c - \frac{1}{2}\Phi_E}{\Phi_0}\right) \\ &= -E_J \cos\left(\pi \frac{\Phi_E}{\Phi_0}\right) \left[\cos\left(2\pi \frac{\phi_1}{\Phi_0}\right) \cos\left(2\pi \frac{\phi_c}{\Phi_0}\right) + \sin\left(2\pi \frac{\phi_1}{\Phi_0}\right) \sin\left(2\pi \frac{\phi_c}{\Phi_0}\right) \right] \\ &+ E_J d \sin\left(\pi \frac{\Phi_E}{\Phi_0}\right) \left[-\cos\left(2\pi \frac{\phi_1}{\Phi_0}\right) \sin\left(2\pi \frac{\phi_c}{\Phi_0}\right) + \sin\left(2\pi \frac{\phi_1}{\Phi_0}\right) \cos\left(2\pi \frac{\phi_c}{\Phi_0}\right) \right]. \end{aligned} \quad (\text{A18})$$

Now, the total Hamiltonian of the system can be written as

$$\begin{aligned} \mathcal{H} &= 4E_C(n - n_g)^2 + 4E_C \left(\frac{C_{\Sigma 12}^2}{C_{\Sigma 1} C_{\Sigma 2}} - 1 \right) n_g^2 \\ &+ \frac{1}{2C_{\Sigma c}} Q_c^2 + \left(\frac{1}{C_{\Sigma 1c}} 2en + \frac{C_{\Sigma 12}}{C_{\Sigma 1} C_{\Sigma 2c}} 2en_g \right) Q_c \\ &- E_J \cos\left(\pi \frac{\Phi_E}{\Phi_0}\right) \left[\cos\left(2\pi \frac{\phi_1}{\Phi_0}\right) \cos\left(2\pi \frac{\phi_c}{\Phi_0}\right) + \sin\left(2\pi \frac{\phi_1}{\Phi_0}\right) \sin\left(2\pi \frac{\phi_c}{\Phi_0}\right) \right] \\ &+ E_J d \sin\left(\pi \frac{\Phi_E}{\Phi_0}\right) \left[-\cos\left(2\pi \frac{\phi_1}{\Phi_0}\right) \sin\left(2\pi \frac{\phi_c}{\Phi_0}\right) + \sin\left(2\pi \frac{\phi_1}{\Phi_0}\right) \cos\left(2\pi \frac{\phi_c}{\Phi_0}\right) \right] \\ &+ \frac{1}{2L_B} \phi_2^2 + \frac{1}{2L_c} \phi_c^2. \end{aligned} \quad (\text{A19})$$

In the limit $C_B \rightarrow \infty$, the definitions introduced in Eqs. (A11) and (A15) simplify to

$$\frac{1}{C_{\Sigma 1}} \rightarrow \frac{C_c + C_J}{C_c C_J + C_{g1}(C_c + C_J)}, \quad (\text{A20a})$$

$$\frac{1}{C_{\Sigma 2}} \rightarrow 0, \quad (\text{A20b})$$

$$\frac{1}{C_{\Sigma c}} \rightarrow \frac{C_{g1} + C_J}{C_c C_J + C_{g1}(C_c + C_J)}, \quad (\text{A20c})$$

$$\frac{1}{C_{\Sigma 1c}} \rightarrow \frac{C_J}{C_c C_J + C_{g1}(C_c + C_J)}, \quad (\text{A20d})$$

$$\frac{1}{C_{\Sigma 12}} \rightarrow 0, \quad (\text{A20e})$$

$$\frac{1}{C_{\Sigma 2c}} \rightarrow 0, \quad (\text{A20f})$$

$$n_g \rightarrow -\frac{C_{g1}}{2e} V_g, \quad (\text{A20g})$$

recovering the result that the gate charge is solely determined by the voltage bias and the gate capacitor.

APPENDIX B: DERIVING THE EFFECTIVE CAPACITANCE

In the following, we determine the effective capacitance of the CPB part of the circuit. Let us first determine the electric charges on the different islands of the circuit. These arise from the relation in Eq. (A8):

$$Q_1 = \frac{\partial \mathcal{L}}{\partial \phi_1} = (C_J + C_{g1}) \dot{\phi}_1 - C_{g1} \dot{\phi}_2 - C_J \dot{\phi}_c, \quad (\text{B1a})$$

$$Q_2 = \frac{\partial \mathcal{L}}{\partial \phi_2} = (C_{g1} + C_{g2} + C_B) \dot{\phi}_2 - C_{g1} \dot{\phi}_1, \quad (\text{B1b})$$

$$Q_c = \frac{\partial \mathcal{L}}{\partial \phi_3} = (C_c + C_J) \dot{\phi}_c - C_{g1} \dot{\phi}_1. \quad (\text{B1c})$$

Recall the definition of V_g in Eq. (A13). In the large C_B limit, $C_{\Sigma 2} \rightarrow C_B$, and together with the relation Eq. (B1b), $\phi_2 = V_g$ is implied. Now that the voltage on the island is fixed to V_g in this limit, the number of Cooper pairs on island 1 can be determined by combining the relations Eqs. (A15b) and (B1a):

$$n = \frac{Q_1}{2e} = \frac{(C_J + C_{g1}) \dot{\phi}_1 - C_{g1} \dot{\phi}_2 - C_J \dot{\phi}_c}{2e}. \quad (\text{B2})$$

The voltage on the CPB island is thus

$$V_I = \dot{\phi}_I = \frac{C_{g1}}{C_J + C_{g1}} V_g + \frac{2en}{C_J + C_{g1}} + \frac{C_J}{C_J + C_{g1}} \dot{\phi}_c \quad (\text{B3})$$

and, therefore, the charge across C_{g1} can be written

$$Q_{g1} = C_{g1}(V_g - V_I) = \frac{C_J C_{g1}}{C_J + C_{g1}} V_g - \frac{C_{g1}}{C_J + C_{g1}} 2en - \frac{C_J C_{g1}}{C_J + C_{g1}} \dot{\phi}_c. \quad (\text{B4})$$

Notice that here the second term has the opposite sign compared to the calculation presented by Duty *et al.* [29]. However, our gate charge is also defined with the opposite sign with respect to the gate voltage, see Eq. (A20g). Thus the effective capacitance [Eq. (2) in the main text] obtained here aligns with the results in Ref. [29],

$$C_{\text{eff}} = \frac{\partial Q_{g1}}{\partial V_g} = \frac{C_{g1} C_J}{C_{g1} + C_J} - \frac{C_{g1}^2}{4e^2} \frac{\partial^2 E_k}{\partial n_g^2}, \quad (\text{B5})$$

where E_k is the k th energy band of the CPB. We do not have to take the position dependence of C_{g1} into consideration in this part of the derivation. Since we are considering a voltage bias setup with a resonance frequency well below RC cutoff effects, the voltage on the CPB island is able to follow the movement of the capacitor without difficulties.

APPENDIX C: RADIATION PRESSURE AND CROSS-KERR COUPLINGS

Consider the resonance frequency of an LC circuit

$$\omega_c = \frac{1}{\sqrt{L_c C_{\text{tot}}}}, \quad (\text{C1})$$

where the total capacitance C_{tot} arises from the cavity capacitor that is parallel with the second gate capacitor and the effective CPB capacitor

$$C_{\text{tot}} = C_c + \left(\frac{1}{C_{g2}} + \frac{1}{C_{\text{eff}}} \right)^{-1}. \quad (\text{C2})$$

$$\hbar g_{\text{rp}} = \hbar x_{\text{zp}} \left[\frac{1}{2} \frac{C_{g2}^2}{(C_{g2} + C_{\text{eff}})^2} \frac{\omega_c}{C_{\text{tot}}} \right] \left[\frac{C_J^2 C_{g1}'}{(C_{g1} + C_J)^2} - \frac{C_{g1} C_{g1}'}{2e^2} \frac{\partial^2 E_k}{\partial n_g^2} + \frac{C_{g1}^2 C_{g1}'}{8e^3} V_g \frac{\partial^3 E_k}{\partial n_g^3} \right] \quad (\text{C9})$$

by plugging Eqs. (C5) and (C8) back to (C4).

Conversely, the CK coupling arises from $\hbar \frac{1}{2} \frac{\partial^2 \omega_c}{\partial x^2} \hat{x}^2$, leading to

$$\hbar g_{\text{CK}} = \frac{1}{2} \hbar \frac{\partial^2 \omega_c}{\partial x^2} x_{\text{zp}}^2. \quad (\text{C10})$$

A direct calculation leads to

$$\begin{aligned} \frac{\partial^2 \omega_c}{\partial x^2} &= \omega_c C_{g2}^2 \frac{C_{g2}(4C_c + 3C_{g2}) + 4(C_c + C_{g2})C_{\text{eff}}}{4(C_{g2} + C_{\text{eff}})^2 [C_c C_{g2} + (C_c + C_{g2})C_{\text{eff}}]^2} \left(\frac{\partial C_{\text{eff}}}{\partial x} \right)^2 \\ &\quad - \omega_c C_{g2}^2 \frac{1}{2(C_{g2} + C_{\text{eff}})[C_c C_{g2} + (C_c + C_{g2})C_{\text{eff}}]} \frac{\partial^2 C_{\text{eff}}}{\partial x^2}, \end{aligned} \quad (\text{C11})$$

The cavity frequency can be expanded in the position of the moving capacitor $C_{g1}(x)$:

$$\omega_c \simeq \omega_{c0} + \frac{\partial \omega_c}{\partial x} x + \frac{1}{2} \frac{\partial^2 \omega_c}{\partial x^2} x^2. \quad (\text{C3})$$

Here, the linear term corresponds to the radiation pressure coupling. Thinking about a simple optical cavity, the decrease in cavity length should lead to the increase in cavity frequency. The quantization of the circuit gives the position operator the form $\hat{x} = x_{\text{zp}}(b^\dagger + b)$, where x_{zp} is the zero point motion. Thus the radiation pressure coupling is

$$\hbar g_{\text{rp}} = -\hbar \frac{\partial \omega_c}{\partial x} x_{\text{zp}}. \quad (\text{C4})$$

A straightforward calculation yields

$$\frac{\partial \omega_c}{\partial x} = -\frac{1}{2} \frac{C_{g2}^2}{(C_{g2} + C_{\text{eff}})^2} \frac{\omega_c}{C_{\text{tot}}} \frac{\partial C_{\text{eff}}}{\partial x}, \quad (\text{C5})$$

with

$$\frac{\partial C_{\text{eff}}}{\partial x} = -\frac{C_J^2 C_{g1}'}{(C_{g1} + C_J)^2} - \frac{C_{g1} C_{g1}'}{2e^2} \frac{\partial^2 E_k}{\partial n_g^2} - \frac{C_{g1}^2}{4e^2} \frac{\partial}{\partial x} \left(\frac{\partial^2 E_k}{\partial n_g^2} \right), \quad (\text{C6})$$

arising from the expression Eq. (2). Here the prime notation is used to mark the x derivatives. Using the chain rule, we can determine

$$\frac{\partial}{\partial x} \left(\frac{\partial^2 E_k}{\partial n_g^2} \right) = \frac{\partial n_g}{\partial x} \frac{\partial}{\partial n_g} \left(\frac{\partial^2 E_k}{\partial n_g^2} \right) = -\frac{V_g}{2e} C_{g1}' \frac{\partial^3 E_k}{\partial n_g^3}, \quad (\text{C7})$$

where the gate charge definition Eq. (A20g) is used. Thus we obtain

$$\frac{\partial C_{\text{eff}}}{\partial x} = -\frac{C_J^2 C_{g1}'}{(C_{g1} + C_J)^2} - \frac{C_{g1} C_{g1}'}{2e^2} \frac{\partial^2 E_k}{\partial n_g^2} + \frac{C_{g1}^2 C_{g1}'}{8e^3} V_g \frac{\partial^3 E_k}{\partial n_g^3}, \quad (\text{C8})$$

leading to the radiation pressure coupling [Eq. (5) in the main text]

where

$$\begin{aligned} \frac{\partial^2 C_{\text{eff}}}{\partial x^2} = & -\frac{2C_J C_{g1}^2}{(C_{g1} + C_J)^2} + \frac{C_J C_{g1}''}{C_{g1} + C_J} + C_J C_{g1} \left[\frac{2C_{g1}'^2}{(C_{g1} + C_J)^3} - \frac{C_{g1}''}{(C_{g1} + C_J)^2} \right] \\ & - \frac{1}{4e^2} \left[4C_{g1} C_{g1}' \frac{\partial}{\partial x} \left(\frac{\partial^2 E_k}{\partial n_g^2} \right) + (2C_{g1}'^2 + 2C_{g1} C_{g1}'') \frac{\partial^2 E_k}{\partial n_g^2} + C_{g1}^2 \frac{\partial^2}{\partial x^2} \left(\frac{\partial^2 E_k}{\partial n_g^2} \right) \right]. \end{aligned} \quad (\text{C12})$$

Utilizing the second-order chain rule $\frac{\partial^2 y}{\partial x^2} = \frac{\partial^2 y}{\partial z^2} \left(\frac{\partial z}{\partial x} \right)^2 + \frac{\partial y}{\partial z} \frac{\partial^2 z}{\partial x^2}$, we obtain

$$\begin{aligned} \frac{\partial^2}{\partial x^2} \left(\frac{\partial^2 E_k}{\partial n_g^2} \right) &= \left(\frac{\partial n_g}{\partial x} \right)^2 \frac{\partial^4 E_k}{\partial n_g^4} + \frac{\partial^2 n_g}{\partial x^2} \frac{\partial^3 E_k}{\partial n_g^3} \\ &= \left(-\frac{V_g}{2e} C_{g1}' \right)^2 \frac{\partial^4 E_k}{\partial n_g^4} - \frac{V_g}{2e} C_{g1}'' \frac{\partial^3 E_k}{\partial n_g^3}, \end{aligned} \quad (\text{C13})$$

giving the explicit form of the second derivative

$$\begin{aligned} \frac{\partial^2 C_{\text{eff}}}{\partial x^2} = & -\frac{C_J C_{g1}^2}{(C_{g1} + C_J)^2} + \frac{C_J C_{g1}''}{C_{g1} + C_J} + C_J C_{g1} \left[\frac{2C_{g1}'^2}{(C_{g1} + C_J)^3} - \frac{C_{g1}''}{(C_{g1} + C_J)^2} \right] \\ & - \frac{1}{4e^2} \left[(2C_{g1}'^2 + 2C_{g1} C_{g1}'') \frac{\partial^2 E_k}{\partial n_g^2} - \left(2C_{g1} C_{g1}' \frac{V_g}{e} + C_{g1}^2 C_{g1}'' \frac{V_g}{2e} \right) \frac{\partial^3 E_k}{\partial n_g^3} + C_{g1}^2 \left(-\frac{V_g}{2e} C_{g1}' \right)^2 \frac{\partial^4 E_k}{\partial n_g^4} \right], \end{aligned} \quad (\text{C14})$$

which is the result Eq. (9) in the main text

APPENDIX D: QUANTIZING THE HAMILTONIAN

Let us divide the full Hamiltonian Eq. (A19) into parts. The cavity, mechanics, cavity-mechanics-CPB coupling, charging, and Josephson-junction sub-Hamiltonians are

$$\mathcal{H} = \mathcal{H}_c + \mathcal{H}_m + \mathcal{H}_{\text{cm}} + \mathcal{H}_{\text{ch}} + \mathcal{H}_{\text{JJ}}, \quad (\text{D1a})$$

$$\mathcal{H}_c = \frac{1}{2C_{\Sigma c}} Q_c^2 + \frac{1}{2L_c} \phi_c^2, \quad (\text{D1b})$$

$$\mathcal{H}_m = 4E_C \left(\frac{C_{\Sigma 12}^2}{C_{\Sigma 1} C_{\Sigma 2}} - 1 \right) n_g^2, \quad (\text{D1c})$$

$$\mathcal{H}_{\text{cm}} = \frac{C_{\Sigma 12}}{C_{\Sigma 1} C_{\Sigma 2c}} 2en_g Q_c, \quad (\text{D1d})$$

$$\mathcal{H}_{\text{ch}} = 4E_C (n - n_g)^2 + \frac{1}{C_{\Sigma 1c}} 2en_g Q_c, \quad (\text{D1e})$$

$$\begin{aligned} \mathcal{H}_{\text{JJ}} = & -E_J \cos \left(\pi \frac{\Phi_E}{\Phi_0} \right) [\cos(\varphi_1) \cos(\varphi_c) \\ & + \sin(\varphi_1) \sin(\varphi_c)] + E_J d \sin \left(\pi \frac{\Phi_E}{\Phi_0} \right) \\ & \times [-\cos(\varphi_1) \sin(\varphi_c) + \sin(\varphi_1) \cos(\varphi_c)]. \end{aligned} \quad (\text{D1f})$$

1. Cavity Hamiltonian

Let us first quantize the cavity Hamiltonian Eq. (D1b). Quantized cavity flux and its conjugate momentum (charge) fulfill the canonical commutation relation

$$[\hat{\phi}_c, \hat{Q}_c] = i\hbar, \quad (\text{D2})$$

and introduce bosonic operators \hat{a}, \hat{a}^\dagger with $[\hat{a}, \hat{a}^\dagger] = 1$ so

$$\hat{\phi}_c = \Phi_{zp} (\hat{a} + \hat{a}^\dagger), \quad (\text{D3a})$$

$$\hat{Q}_c = -iQ_{zp} (\hat{a} - \hat{a}^\dagger). \quad (\text{D3b})$$

Applying these to the canonical commutation relation Eq. (D2) implies

$$2\Phi_{zp} Q_{zp} = \hbar. \quad (\text{D4})$$

Thus we can rewrite the quantized cavity Hamiltonian

$$\begin{aligned} \hat{\mathcal{H}}_c = & \left(\frac{Q_{zp}^2}{C_{\Sigma c}} + \frac{\Phi_{zp}^2}{L_c} \right) \left(\hat{a}^\dagger \hat{a} + \frac{1}{2} \right) + \left(-\frac{Q_{zp}^2}{2C_{\Sigma c}} + \frac{\Phi_{zp}^2}{2L_c} \right) \\ & \times (\hat{a}^2 + \hat{a}^{\dagger 2}), \end{aligned} \quad (\text{D5})$$

where we can denote $\hbar\omega_c = \frac{Q_{zp}^2}{C_{\Sigma c}} + \frac{\Phi_{zp}^2}{L_c}$. Φ_{zp} and Q_{zp} can be solved from this using the relation Eq. (D4) and the standard way of writing the cavity angular frequency:

$$\omega_c = \frac{1}{\sqrt{L_c C_{\Sigma c}}}. \quad (\text{D6})$$

We find that

$$Q_{zp} = \sqrt{\frac{\hbar}{2Z_0}}, \quad (\text{D7a})$$

$$\Phi_{zp} = \sqrt{\frac{\hbar Z_0}{2}}, \quad (\text{D7b})$$

$$Z_0 = \sqrt{\frac{L_c}{C_{\Sigma c}}}, \quad (\text{D7c})$$

and thus the cavity Hamiltonian can be written

$$\hat{\mathcal{H}}_c = \hbar\omega_c \left(\hat{a}^\dagger \hat{a} + \frac{1}{2} \right), \quad (\text{D8})$$

where the constant term can be neglected without loss of generality.

Recall that in Eq. (D6) we have a position-dependent capacitance $C_{\Sigma c}$. Thus we obtain a direct optomechanical coupling that is not enhanced by the qubit similar to the terms not

involving derivatives of the qubit energy bands in the circuit approach. A straightforward calculation yields us the result Eq. (12a) in the main text,

$$\tilde{g}_{\text{tpd}} = -\frac{\partial \omega_c}{\partial x} x_{\text{zp}} = \frac{\omega_{c0}}{2C_{\Sigma c}} \frac{C_J^2 C'_{g1}}{(C_J + C_{g1})^2} x_{\text{zp}}, \quad (\text{D9})$$

and similarly for the direct CK coupling

$$\begin{aligned} \tilde{g}_{\text{CKd}} = \frac{1}{2} \frac{\partial^2 \omega_c}{\partial x^2} x_{\text{zp}}^2 = \frac{1}{2} \left[\frac{3\omega_{c0}}{4C_{\Sigma c}^2} \left(\frac{C_J^2 C'_{g1}}{(C_J + C_{g1})^2} \right)^2 \right. \\ \left. - \frac{\omega_{c0} C_J^2}{2C_{\Sigma c}} \left(\frac{-2C_{g1}'^2 + (C_J + C_{g1}) C'_{g1}}{(C_J + C_{g1})^3} \right) \right] x_{\text{zp}}^2, \quad (\text{D10}) \end{aligned}$$

i.e., Eq. (12b) in the main text.

A simple calculation shows that the direct optomechanical couplings from the circuit method Eqs. (C9) and (C10) align with the corresponding quantum mechanical results Eqs. (12a) and (12b) when C_{g2} is large. From the circuit model, the direct couplings are obtained by ignoring the energy band terms, i.e., setting $E_J = 0$.

2. Mechanics Hamiltonian

The mechanics Hamiltonian Eq. (D1c) can be quantized in a similar fashion. Notice that the gate charge n_g is displacement x dependent as the capacitance $C_{g1}(x)$ depends on the separation of the gate electrodes. We approximate

$$n_g \approx n_{g0} + \frac{\partial n_g}{\partial x} x, \quad (\text{D11})$$

and using the definition of n_g Eq. (A20g), we find

$$\frac{\partial n_g}{\partial x} = -\frac{C'_{g1}}{2e} V_g. \quad (\text{D12})$$

By defining bosonic operators for the mechanics \hat{b}, \hat{b}^\dagger with $[\hat{b}, \hat{b}^\dagger] = 1$, we may quantize the displacement as

$$\hat{x} = x_{\text{zp}}(\hat{b} + \hat{b}^\dagger). \quad (\text{D13})$$

The quantized mechanics Hamiltonian is thus (neglecting constants)

$$\begin{aligned} \hat{\mathcal{H}}_m = 4E_C \left(\frac{C_{\Sigma 12}^2}{C_{\Sigma 1} C_{\Sigma 2}} - 1 \right) \left[2 \left(\frac{\partial n_g}{\partial x} \right)^2 x_{\text{zp}}^2 \hat{b}^\dagger \hat{b} \right. \\ \left. + 2n_g \frac{\partial n_g}{\partial x} x_{\text{zp}} (\hat{b}^\dagger + \hat{b}) + \left(\frac{\partial n_g}{\partial x} \right)^2 x_{\text{zp}}^2 (\hat{b}^{\dagger 2} + \hat{b}^2) \right] \\ = \hbar \omega_m \hat{b}^\dagger \hat{b} + h_1 (\hat{b}^\dagger + \hat{b}) + h_2 (\hat{b}^{\dagger 2} + \hat{b}^2). \quad (\text{D14}) \end{aligned}$$

We now have enough information to also quantize \mathcal{H}_{cm} Eq. (D1d) that directly couples the cavity to the mechanics, and obtain

$$\begin{aligned} \hat{\mathcal{H}}_{\text{cm}} = \frac{C_{\Sigma 12}}{C_{\Sigma 1} C_{\Sigma 2c}} \cdot 2e \left(n_{g0} + \frac{\partial n_g}{\partial x} \hat{x} \right) \hat{Q}_c \\ = -i2e \frac{C_{\Sigma 12}}{C_{\Sigma 1} C_{\Sigma 2c}} \left[n_{g0} - \frac{C'_{g1}}{2e} V_g x_{\text{zp}} (\hat{b} + \hat{b}^\dagger) \right] \hat{Q}_{\text{zp}} (\hat{a} - \hat{a}^\dagger). \quad (\text{D15}) \end{aligned}$$

This term is, however, omitted in the discussion since the cavity-mechanics coupling arising from it is not of the radiation pressure or CK form.

3. Josephson junction Hamiltonian

To quantize the Josephson junction Hamiltonian Eq. (D1f), let us first discuss how the phase on the CPB island relates to the qubit operations when the tunneling junctions are considered as two-level systems. The following derivation closely follows the treatment of tunnel junctions by Vool and Devoret [42]. The tunneling Hamiltonian of a Josephson junction can be written in a number basis using the transmitted charge through the junction, which in terms of Cooper pairs reads as

$$\hat{\mathcal{H}}_T = -\frac{E_T}{2} \sum_{N=-\infty}^{N=\infty} [|N\rangle \langle N+1| + |N+1\rangle \langle N|], \quad (\text{D16})$$

where the tunneling energy is denoted by E_T . This number basis representation can be related to the alternate phase basis by equations

$$|\varphi\rangle = \sum_{N=-\infty}^{\infty} e^{iN\varphi} |N\rangle, \quad (\text{D17a})$$

$$|N\rangle = \frac{1}{2\pi} \int_0^{2\pi} d\varphi e^{-iN\varphi} |\varphi\rangle. \quad (\text{D17b})$$

A straightforward calculation reveals that the operator

$$e^{i\hat{\varphi}} = \frac{1}{2\pi} \int_0^{2\pi} d\phi e^{i\phi} |\varphi\rangle \langle \varphi| \quad (\text{D18})$$

has the following translation properties:

$$e^{i\hat{\varphi}} |N\rangle = |N-1\rangle, \quad (\text{D19a})$$

$$e^{-i\hat{\varphi}} |N\rangle = |N+1\rangle. \quad (\text{D19b})$$

Confining our approach to a two-level setting, i.e., we only consider qubit states $|0\rangle$ and $|1\rangle$, directly leads to

$$\cos \hat{\varphi} = \frac{1}{2} [e^{i\hat{\varphi}} + e^{-i\hat{\varphi}}] = \frac{1}{2} [|1\rangle \langle 0| + |0\rangle \langle 1|] = \frac{1}{2} \sigma_x, \quad (\text{D20a})$$

$$\sin \hat{\varphi} = \frac{1}{2i} [e^{i\hat{\varphi}} - e^{-i\hat{\varphi}}] = \frac{i}{2} [|1\rangle \langle 0| - |0\rangle \langle 1|] = -\frac{1}{2} \sigma_y. \quad (\text{D20b})$$

We may thus identify

$$\cos(\hat{\varphi}_1) = \frac{1}{2} \sigma_x, \quad (\text{D21a})$$

$$\sin(\hat{\varphi}_1) = -\frac{1}{2} \sigma_y, \quad (\text{D21b})$$

where $\sigma_{x,y}$ are the Pauli matrices with conventions

$$\sigma_x = |1\rangle \langle 0| + |0\rangle \langle 1| = \begin{pmatrix} 0 & 1 \\ 1 & 0 \end{pmatrix}, \quad (\text{D22a})$$

$$\sigma_y = i(|0\rangle \langle 1| - |1\rangle \langle 0|) = i \begin{pmatrix} 0 & -1 \\ 1 & 0 \end{pmatrix}, \quad (\text{D22b})$$

$$|0\rangle = \begin{pmatrix} 0 \\ 1 \end{pmatrix}, \quad (\text{D22c})$$

$$|1\rangle = \begin{pmatrix} 1 \\ 0 \end{pmatrix}. \quad (\text{D22d})$$

By recalling the cavity flux operator Eq. (D3a) and the phase-flux relation $\varphi_c = 2\pi \frac{\varphi_c}{\Phi_0}$, we can write

$$\hat{\varphi}_c = \eta(\hat{a} + \hat{a}^\dagger), \quad (\text{D23a})$$

$$\eta = \sqrt{\frac{2e^2 Z_0}{\hbar}}. \quad (\text{D23b})$$

We can expand the trigonometric functions of the cavity flux operators in the JJ Hamiltonian Eq. (D1f):

$$\sin(\hat{\varphi}_c) \approx \hat{\varphi}_c = \eta(\hat{a} + \hat{a}^\dagger), \quad (\text{D24a})$$

$$\cos(\hat{\varphi}_c) \approx 1 - \frac{1}{2}\hat{\varphi}_c^2 = 1 - \frac{1}{2}\eta^2(\hat{a} + \hat{a}^\dagger)^2. \quad (\text{D24b})$$

Taking the lowest order approximation of the trigonometric functions is an important limiting factor of the accuracy of the quantum mechanical approach to the circuit dynamics. This allows only very small values of η , i.e., small values of Z_0 , to be considered. Higher order approximation would improve the accuracy of the results compared to the circuit method but our aim here is only to highlight the intermediate steps of the quantum mechanical calculation.

Now the Josephson junction Hamiltonian simplifies to

$$\begin{aligned} \hat{\mathcal{H}}_{\text{JJ}} &= -\frac{E_J}{2} \left[\cos\left(\pi \frac{\Phi_E}{\Phi_0}\right) \sigma_x + d \sin\left(\pi \frac{\Phi_E}{\Phi_0}\right) \sigma_y \right] \\ &+ \frac{E_J}{2} \left[\cos\left(\pi \frac{\Phi_E}{\Phi_0}\right) \sigma_y - d \sin\left(\pi \frac{\Phi_E}{\Phi_0}\right) \sigma_x \right] \eta(\hat{a} + \hat{a}^\dagger) \\ &+ \frac{E_J}{4} \left[\cos\left(\pi \frac{\Phi_E}{\Phi_0}\right) \sigma_x + d \sin\left(\pi \frac{\Phi_E}{\Phi_0}\right) \sigma_y \right] \eta^2(\hat{a} + \hat{a}^\dagger)^2 \\ &= -\frac{B_1}{2} \sigma_x - \frac{B_2}{2} \sigma_y + g_1 \sigma_y \hat{x}_c + g_2 \sigma_x \hat{x}_c^2 + g_3 \sigma_x \hat{x}_c + g_4 \sigma_y \hat{x}_c^2, \end{aligned} \quad (\text{D25})$$

with

$$B_1 = E_J \cos\left(\pi \frac{\Phi_E}{\Phi_0}\right), \quad (\text{D26a})$$

$$B_2 = E_J d \sin\left(\pi \frac{\Phi_E}{\Phi_0}\right), \quad (\text{D26b})$$

$$g_1 = \frac{B_1}{2} \eta, \quad (\text{D26c})$$

$$g_2 = \frac{B_1}{4} \eta^2, \quad (\text{D26d})$$

$$g_3 = -\frac{B_2}{2} \eta, \quad (\text{D26e})$$

$$g_4 = \frac{B_2}{4} \eta^2, \quad (\text{D26f})$$

$$\hat{x}_c = \hat{a} + \hat{a}^\dagger. \quad (\text{D26g})$$

In the limit $d \rightarrow 0$, i.e., symmetric Josephson junctions, Eq. (17) in the main text is obtained.

4. Charging Hamiltonian

The full charging Hamiltonian Eq. (D1e) can be written in a quantized form

$$\hat{\mathcal{H}}_{\text{ch}} = \sum_n \left[4E_C (\hat{n} - n_g)^2 + \frac{2e}{C_{\Sigma 1c}} \hat{n} \hat{Q}_c \right] |n\rangle \langle n|. \quad (\text{D27})$$

To obtain the result Eq. (13) in the main text, we omit the second term with the cavity charge \hat{Q}_c since we restrict ourselves to a low-frequency analysis of the circuit. The neglected term is of the form $\sim -i2en\omega_c \Phi_{zp}(\hat{a} - \hat{a}^\dagger)$, essentially coupling the voltage of the cavity to the qubit charge. With low enough cavity resonance frequencies, this term is not significant and including it would only result in unnecessary algebraic complications in the perturbation theory approach that we use to estimate the quantum mechanical couplings due to it not commuting with other terms in the Hamiltonian. The eigenenergies are thus $E_n = 4E_C(n - n_g)^2$ parabolas as the function of n_g . Assuming that $E_J \ll E_C$, the contribution from the JJ Hamiltonian Eq. (D25) to the qubit energy is negligible and the total qubit energy can be approximated with the parabolas E_n .

Denote $n_{g0} = \text{int}(n_{g0}) + \delta n_{g0}$ with $\delta n_{g0} \in [0, 1]$ and concentrate on the states closest to n_{g0} , i.e., $n = \text{int}(n_{g0})$ and $n = \text{int}(n_{g0}) + 1$, and call these states $|0\rangle$ and $|1\rangle$, respectively. From E_n , we can see that the degeneracy point of this well-defined qubit is at $n_g = \frac{1}{2}$.

Thus, in the two-level system approximation, the charging Hamiltonian is

$$\begin{aligned} \hat{\mathcal{H}}_{\text{ch}} &= 2E_C(1 - 2\delta n_{g0})\sigma_z \\ &= 2E_C(1 - 2\delta n_{g0})\sigma_z - 4E_C \frac{\partial n_g}{\partial x} \hat{x} \sigma_z \\ &= -\frac{B_3}{2} \sigma_z - g_m \hat{x}_m \sigma_z, \end{aligned} \quad (\text{D28})$$

where

$$B_3 = -4E_C(1 - 2\delta n_{g0}), \quad (\text{D29a})$$

$$g_m = 4E_C \frac{\partial n_g}{\partial x} x_{zp} = 4E_C \left(-\frac{1}{2e} C'_{g1} V_g \right)$$

$$x_{zp} = -\frac{2}{e} E_C V_g C'_{g1} x_{zp}, \quad (\text{D29b})$$

$$\hat{x}_m = \hat{b} + \hat{b}^\dagger. \quad (\text{D29c})$$

APPENDIX E: PERTURBATIVE APPROACH TO THE QUBIT

Let us regroup the quantized Hamiltonians based on their effects on the qubit,

$$\hat{\mathcal{H}} = \hat{\mathcal{H}}_0 + \hat{\mathcal{H}}_x + \hat{\mathcal{H}}_y + \hat{\mathcal{H}}_z, \quad (\text{E1a})$$

$$\hat{\mathcal{H}}_0 = \hat{\mathcal{H}}_c + \hat{\mathcal{H}}_m + \hat{\mathcal{H}}_{\text{cm}}, \quad (\text{E1b})$$

$$\hat{\mathcal{H}}_x = \left[-\frac{1}{2}B_1 + g_3 \hat{x}_c + g_2 \hat{x}_c^2 \right] \sigma_x = -\frac{1}{2} \tilde{B}_1 \sigma_x, \quad (\text{E1c})$$

$$\hat{\mathcal{H}}_y = \left[-\frac{1}{2}B_2 + g_1 \hat{x}_c + g_4 \hat{x}_c^2 \right] \sigma_y = -\frac{1}{2} \tilde{B}_2 \sigma_y, \quad (\text{E1d})$$

$$\hat{\mathcal{H}}_z = \left[-\frac{1}{2}B_3 - g_m \hat{x}_m \right] \sigma_z = -\frac{1}{2} \tilde{B}_3 \sigma_z, \quad (\text{E1e})$$

with

$$\tilde{B}_1 = B_1 - 2g_3 \hat{x}_c - 2g_2 \hat{x}_c^2, \quad (\text{E2a})$$

$$\tilde{B}_2 = B_2 - 2g_1 \hat{x}_c - 2g_4 \hat{x}_c^2, \quad (\text{E2b})$$

$$\tilde{B}_3 = B_3 + 2g_m \hat{x}_m. \quad (\text{E2c})$$

Provided that $E_C \gg E_J$, the additional terms in \tilde{B}_j can be considered as a small perturbation to the unperturbed qubit

Hamiltonian

$$\hat{H}_{Q0} = -\frac{1}{2}(B_1\sigma_x + B_2\sigma_y + B_3\sigma_z). \quad (\text{E3})$$

We can treat our system with a perturbation approach to the \hat{H}_{Q0} with eigenenergies $\pm\frac{1}{2}\sqrt{B_1^2 + B_2^2 + B_3^2}$. Thus we can approximate the full Hamiltonian as a perturbation to the qubit ground state

$$\hat{H} = \hat{H}_0 - \frac{1}{2}\sqrt{\tilde{B}_1^2 + \tilde{B}_2^2 + \tilde{B}_3^2}. \quad (\text{E4})$$

Let us write in the above expression explicitly

$$\begin{aligned} & -\frac{1}{2}\sqrt{\tilde{B}_1^2 + \tilde{B}_2^2 + \tilde{B}_3^2} \\ &= -\frac{1}{2}B\sqrt{1 + \frac{1}{B^2}(\alpha\hat{x}_c + \beta\hat{x}_c^2 + \rho\hat{x}_c^3 + \delta\hat{x}_c^4 + \epsilon\hat{x}_m + \lambda\hat{x}_m^2)}, \end{aligned} \quad (\text{E5})$$

with

$$B = \sqrt{B_1^2 + B_2^2 + B_3^2}, \quad (\text{E6a})$$

$$\alpha = -4(B_1g_3 + B_2g_1) = 0, \quad (\text{E6b})$$

$$\beta = 4(g_3^2 + g_1^2 - B_1g_2 - B_2g_4) = 0, \quad (\text{E6c})$$

$$\rho = 8(g_2g_3 + g_1g_4) = 0, \quad (\text{E6d})$$

$$\delta = 4(g_2^2 + g_4^2), \quad (\text{E6e})$$

$$\epsilon = 4B_3g_m, \quad (\text{E6f})$$

$$\lambda = 4g_m^2. \quad (\text{E6g})$$

Recall that $\sqrt{1+x} \approx 1 + \frac{x}{2} - \frac{x^2}{8} + \frac{x^3}{16}$, which allows us to expand the above expression provided that B is large, i.e., E_C is large:

$$\begin{aligned} & -\frac{1}{2}\sqrt{\tilde{B}_1^2 + \tilde{B}_2^2 + \tilde{B}_3^2} \\ & \approx -\frac{1}{2}B - \frac{1}{4B}(\delta\hat{x}_c^4 + \epsilon\hat{x}_m + \lambda\hat{x}_m^2) \\ & + \frac{1}{16B^3}(\delta\hat{x}_c^4 + \epsilon\hat{x}_m + \lambda\hat{x}_m^2)^2 \\ & - \frac{1}{32B^5}(\delta\hat{x}_c^4 + \epsilon\hat{x}_m + \lambda\hat{x}_m^2)^3. \end{aligned} \quad (\text{E7})$$

We can now identify the terms contributing the radiation pressure coupling ($\hat{x}_c^{2k}\hat{x}_m^{2l+1}$), CK coupling ($\hat{x}_c^{2k}\hat{x}_m^{2l}$). We also need to take into account the prefactors arising from normal ordering the terms contributing to these couplings $\hat{a}^\dagger\hat{a}(\hat{b}^\dagger + \hat{b})$, $\hat{a}^\dagger\hat{a}(\hat{b} + \hat{b}^\dagger)^2$, respectively.

The qubit-mediated part of the radiation pressure coupling [Eq. (23) of the main text] is thus

$$\hbar\tilde{g}_{\text{rpp}} = \frac{\delta\epsilon}{4B^5}\{-6B^2 + 315\delta + 27\lambda\}. \quad (\text{E8})$$

Here we have an extra minus sign fixing the radiation pressure coupling to $g_{\text{rp}} = -\frac{\partial\omega_c}{\partial x}$, i.e., $\hbar\omega_c(x)\hat{a}^\dagger\hat{a} \approx \hbar(\omega_c - g_{\text{rp}}\hat{x}_m)\hat{a}^\dagger\hat{a}$. Finally, the qubit-mediated part of CK coupling [Eq. (24) of

the main text] is

$$\hbar\tilde{g}_{\text{CKp}} = -\frac{1}{2}\frac{\delta}{8B^5}\{-24B^2\lambda + 1260\delta\lambda + 18\epsilon^2 + 108\lambda^2\}. \quad (\text{E9})$$

Now the full optomechanical couplings are obtained from the direct couplings Eqs. (D9), (D10), and the qubit mediated couplings Eqs. (E8) and (E9) as $\tilde{g}_{\text{rp}} = \tilde{g}_{\text{rpd}} + \tilde{g}_{\text{rpp}}$ and $\tilde{g}_{\text{CK}} = \tilde{g}_{\text{CKd}} + \tilde{g}_{\text{CKp}}$.

The third-order expansion for the radiation pressure coupling is not crucial for the result to align well with the circuit model far away from the degeneracy point of the qubit. However, for the CK coupling, expanding to third order offers much better results compared to the circuit model than just the second-order expansion, the third order being the lowest approximation with complete qualitative agreement between the circuit and QM models. The second-order expansion of the CK coupling only captures the maximum amplification at the degeneracy point but the side peaks on both sides of the maximum enhanced coupling are missing.

In Fig. 5(a), we see that the radiation pressure coupling arising from the perturbative quantum mechanical method coincides with the result from the circuit model far away from the degeneracy point of the qubit. Similarly, in Fig. 5(b), results for the CK couplings from the two approach each other far away from the degeneracy point. The accuracy of the QM perturbation approach relies on the magnitude of the expansion parameter $\frac{1}{B^2}(\delta\hat{x}_c^4 + \epsilon\hat{x}_m + \lambda\hat{x}_m^2)$ being small. However, this parameter reaches its maximum values, i.e., the approximation of the qubit ground-state energy has its largest inaccuracy, in the domain of $\delta n_{g0} \sim 0.5$, where the enhancement maxima of the optomechanical couplings are obtained. This contributes to the quantitative difference between the circuit and QM approaches in the vicinity of the degeneracy point of the qubit. Besides the n_g tunability, magnitude of the expansion parameter depends on multiple system parameters and the validity of the expansion should be checked on a case by case basis. The circuit method, therefore, provides a more reliable picture in terms of the quantitative predictions when discussing the charge tuning regime that is relevant in obtaining the maximum enhancement of the optomechanical couplings.

Going to the limit $E_j \ll E_C$ significantly improves the agreement until at $E_j = 0$ one obtains the same limiting direct couplings from the two methods. A better agreement between the circuit approach and the quantum mechanical calculation is also achieved for small V_g and Z_0 . Reducing V_g overall decreases the optomechanical couplings, and for small cavity impedance Z_0 , the term $\frac{2e}{C_{\Sigma 1c}}\hat{n}\hat{Q}_c$ in the charging Hamiltonian Eq. (D27) describing the effect that the cavity voltage has on the charge of the qubit becomes less significant and the approximation that we have performed in omitting it becomes better justified. The radiation pressure couplings from the classical circuit and QM approaches converge faster to the same value when reducing E_j than the CK couplings due to the CK coupling being a higher order effect than our perturbative approach just barely captures, as discussed above. Going to the next higher order in the perturbation theory would also result in faster convergence for the CK couplings.

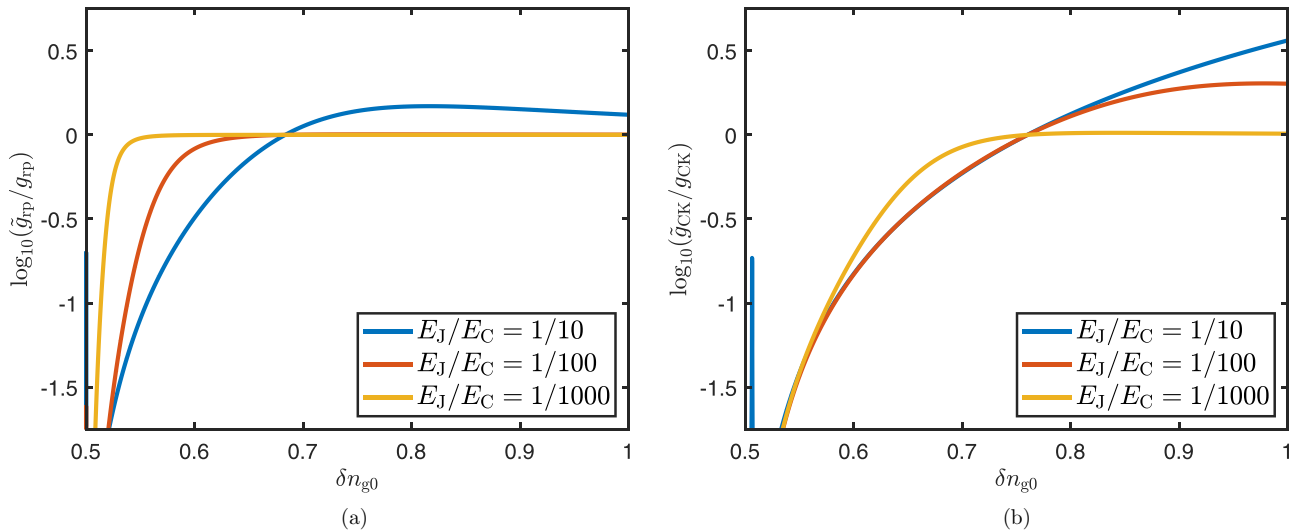


FIG. 5. (a) Comparison between radiation pressure coupling from the quantum mechanical perturbation theory and the circuit model. Ratio between them approaches 1 far away from charge degeneracy points as E_J/E_C ratio becomes smaller. (b) Similar comparison for the CK couplings obtained from the two approaches. Here $V_g = 1$ V and $Z_0 = 1$ Ω to showcase a limit with a good agreement between the two approaches due to the significance of the omitted $\frac{2e}{C_{\Sigma 1c}} \hat{n} \hat{Q}_c$ term from the charging Hamiltonian Eq. (D27) becoming negligible with smaller cavity impedance. The ratios diverting from 1 closer to the degeneracy point of the qubit are due to the maximum enhancement being achieved at slightly different bias points and small difference in the widths of the enhancement peaks in the two methods. Also the parameter used to expand the ground-state energy of the qubit in the QM approach reaches its maximum value close to the degeneracy point, increasing the inaccuracy of the perturbation approach in this regime. $E_C/h = 10$ GHz is fixed in these simulations.

- [1] M. Aspelmeyer, T. J. Kippenberg, and F. Marquardt, Cavity optomechanics, *Rev. Mod. Phys.* **86**, 1391 (2014).
- [2] A. D. Armour, M. P. Blencowe, and K. C. Schwab, Entanglement and Decoherence of a Micromechanical Resonator via Coupling to a Cooper-Pair Box, *Phys. Rev. Lett.* **88**, 148301 (2002).
- [3] C. A. Regal, J. D. Teufel, and K. W. Lehnert, Measuring nanomechanical motion with a microwave cavity interferometer, *Nat. Phys.* **4**, 555 (2008).
- [4] M. D. LaHaye, J. Suh, P. M. Echternach, K. C. Schwab, and M. L. Roukes, Nanomechanical measurements of a superconducting qubit, *Nature (London)* **459**, 960 (2009).
- [5] T. Rocheleau, T. Ndukum, C. Macklin, J. B. Hertzberg, A. A. Clerk, and K. C. Schwab, Preparation and detection of a mechanical resonator near the ground state of motion, *Nature (London)* **463**, 72 (2010).
- [6] J. D. Teufel, T. Donner, D. Li, J. W. Harlow, M. S. Allman, K. Cicak, A. J. Sirois, J. D. Whittaker, K. W. Lehnert, and R. W. Simmonds, Sideband cooling of micromechanical motion to the quantum ground state, *Nature (London)* **475**, 359 (2011).
- [7] P. D. Nation, J. Suh, and M. P. Blencowe, Ultrastrong optomechanics incorporating the dynamical Casimir effect, *Phys. Rev. A* **93**, 022510 (2016).
- [8] L. Neumeier, T. E. Northup, and D. E. Chang, Reaching the optomechanical strong-coupling regime with a single atom in a cavity, *Phys. Rev. A* **97**, 063857 (2018).
- [9] L. Neumeier and D. E. Chang, Exploring unresolved sideband, optomechanical strong coupling using a single atom coupled to a cavity, *New J. Phys.* **20**, 083004 (2018).
- [10] A. Settinieri, V. Macrì, A. Ridolfo, O. Di Stefano, A. F. Kockum, F. Nori, and S. Savasta, Dissipation and thermal noise in hybrid quantum systems in the ultrastrong-coupling regime, *Phys. Rev. A* **98**, 053834 (2018).
- [11] E. Romero-Sánchez, W. P. Bowen, M. R. Vanner, K. Xia, and J. Twamley, Quantum magnetomechanics: Towards the ultrastrong coupling regime, *Phys. Rev. B* **97**, 024109 (2018).
- [12] J.-Q. Liao, J.-F. Huang, L. Tian, L.-M. Kuang, and C.-P. Sun, Generalized ultrastrong optomechanical-like coupling, *Phys. Rev. A* **101**, 063802 (2020).
- [13] M. Kounalakis, Y. M. Blanter, and G. A. Steele, Flux-mediated optomechanics with a transmon qubit in the single-photon ultrastrong-coupling regime, *Phys. Rev. Research* **2**, 023335 (2020).
- [14] S. Ashhab and F. Nori, Qubit-oscillator systems in the ultrastrong-coupling regime and their potential for preparing nonclassical states, *Phys. Rev. A* **81**, 042311 (2010).
- [15] W.-j. Gu, G.-x. Li, S.-p. Wu, and Y.-p. Yang, Generation of nonclassical states of mirror motion in the single-photon strong-coupling regime, *Opt. Express* **22**, 18254 (2014).
- [16] C. Sánchez Muñoz, A. Lara, J. Puebla, and F. Nori, Hybrid Systems for the Generation of Nonclassical Mechanical States via Quadratic Interactions, *Phys. Rev. Lett.* **121**, 123604 (2018).
- [17] I. Marinković, A. Wallucks, R. Riedinger, S. Hong, M. Aspelmeyer, and S. Gröblacher, Optomechanical Bell Test, *Phys. Rev. Lett.* **121**, 220404 (2018).
- [18] C. Ockeloen-Korppi, E. Damskägg, J.-M. Pirkkalainen, M. Asjad, A. A. Clerk, F. Massel, W. M. J., and M. A. Sillanpää, Stabilized entanglement of massive mechanical oscillators, *Nature (London)* **556**, 478 (2018).
- [19] M. H. Devoret, A. Wallraff, and J. M. Martinis, Superconducting qubits a short review, *arXiv:cond-mat/0411174* [cond-mat.mes-hall] (2004).

- [20] M. Abdi, M. Pernpeintner, R. Gross, H. Huebl, and M. J. Hartmann, Quantum State Engineering with Circuit Electromechanical Three-Body Interactions, *Phys. Rev. Lett.* **114**, 173602 (2015).
- [21] O. Shevchuk, G. A. Steele, and Y. M. Blanter, Strong and tunable couplings in flux-mediated optomechanics, *Phys. Rev. B* **96**, 014508 (2017).
- [22] S. Blien, P. Steger, N. Hüttner, R. Graaf, and A. K. Hüttel, Quantum capacitance mediated carbon nanotube optomechanics, *Nat. Commun.* **11**, 1636 (2020).
- [23] T. T. Heikkilä, F. Massel, J. Tuorila, R. Khan, and M. A. Sillanpää, Enhancing Optomechanical Coupling via the Josephson Effect, *Phys. Rev. Lett.* **112**, 203603 (2014).
- [24] A. J. Rimberg, M. P. Blencowe, A. D. Armour, and P. D. Nation, A cavity-Cooper pair transistor scheme for investigating quantum optomechanics in the ultra-strong coupling regime, *New J. Phys.* **16**, 055008 (2014).
- [25] J.-M. Pirkkalainen, S. U. Cho, F. Massel, J. Tuorila, T. T. Heikkilä, P. J. Hakonen, and M. A. Sillanpää, Cavity optomechanics mediated by a quantum two-level system, *Nat. Commun.* **6**, 6981 (2015).
- [26] D. V. Averin, A. B. Zorin, and K. K. Likharev, Bloch oscillations in small Josephson junctions, *Zh. Eksp. Teor. Fiz.* **88**, 692 (1985) [*Sov. Phys. JETP* **61**, 407 (1985)].
- [27] D. V. Averin and C. Bruder, Variable Electrostatic Transformer: Controllable Coupling of Two Charge Qubits, *Phys. Rev. Lett.* **91**, 057003 (2003).
- [28] M. A. Sillanpää, T. Lehtinen, A. Paila, Y. Makhlin, L. Roschier, and P. J. Hakonen, Direct Observation of Josephson Capacitance, *Phys. Rev. Lett.* **95**, 206806 (2005).
- [29] T. Duty, G. Johansson, K. Bladh, D. Gunnarsson, C. Wilson, and P. Delsing, Observation of Quantum Capacitance in the Cooper-Pair Transistor, *Phys. Rev. Lett.* **95**, 206807 (2005).
- [30] F. Persson, C. M. Wilson, M. Sandberg, and P. Delsing, Fast readout of a single Cooper-pair box using its quantum capacitance, *Phys. Rev. B* **82**, 134533 (2010).
- [31] L. Roschier, M. Sillanpää, and P. Hakonen, Quantum capacitive phase detector, *Phys. Rev. B* **71**, 024530 (2005).
- [32] M. D. Shaw, J. Bueno, P. Day, C. M. Bradford, and P. M. Echternach, Quantum capacitance detector: A pair-breaking radiation detector based on the single Cooper-pair box, *Phys. Rev. B* **79**, 144511 (2009).
- [33] N. Imoto, H. A. Haus, and Y. Yamamoto, Quantum nondemolition measurement of the photon number via the optical Kerr effect, *Phys. Rev. A* **32**, 2287 (1985).
- [34] R. Khan, F. Massel, and T. T. Heikkilä, Cross-Kerr nonlinearity in optomechanical systems, *Phys. Rev. A* **91**, 043822 (2015).
- [35] R. Sarala and F. Massel, Cross-Kerr nonlinearity: A stability analysis, *Nanoscale Syst.* **4**, 18 (2015).
- [36] W. Xiong, D.-Y. Jin, Y. Qiu, C.-H. Lam, and J. Q. You, Cross-Kerr effect on an optomechanical system, *Phys. Rev. A* **93**, 023844 (2016).
- [37] S. Chakraborty and A. K. Sarma, Enhancing quantum correlations in an optomechanical system via cross-Kerr nonlinearity, *J. Opt. Soc. Am. B* **34**, 1503 (2017).
- [38] T.-S. Yin, X.-Y. Lü, L.-L. Wan, S.-W. Bin, and Y. Wu, Enhanced photon-phonon cross-Kerr nonlinearity with two-photon driving, *Opt. Lett.* **43**, 2050 (2018).
- [39] M. Kounalakis, C. Dickel, A. Bruno, N. K. Langford, and G. A. Steele, Tuneable hopping and nonlinear cross-Kerr interactions in a high-coherence superconducting circuit, *npj Quantum Inf.* **4**, 38 (2018).
- [40] P. Joyez, P. Lafarge, A. Filipe, D. Esteve, and M. H. Devoret, Observation of Parity-Induced Suppression of Josephson Tunneling in the Superconducting Single Electron Transistor, *Phys. Rev. Lett.* **72**, 2458 (1994).
- [41] J. Aumentado, M. W. Keller, J. M. Martinis, and M. H. Devoret, Nonequilibrium Quasiparticles and $2e$ Periodicity in Single-Cooper-Pair Transistors, *Phys. Rev. Lett.* **92**, 066802 (2004).
- [42] U. Vool and M. H. Devoret, Introduction to quantum electromagnetic circuits, *Int. J. Circ. Theor. Appl.* **45**, 897 (2017).